THE GEOLOGICAL SOCIETY OF AMERICA®

Cenozoic deformation in the eastern domain of the North Qaidam thrust belt, northern Tibetan Plateau

Bing Li[1,2,†], Yongchao Wang[1,2,†], Andrew V. Zuza[3], Xuanhua Chen[1,2], Zhaogang Shao[1,2], Zeng-Zhen Wang[1,2], Yujun Sun[1,2], and Chen Wu[4]

[1]*Chinese Academy of Geological Sciences, Beijing 100037, China*
[2]*Sinoprobe Center, Chinese Academy of Geological Sciences and China Geological Survey, Beijing 100037, China*
[3]*Nevada Bureau of Mines and Geology, University of Nevada, Reno, Nevada 89557, USA*
[4]*Key Laboratory of Continental Collision and Plateau Uplift, Institute of Tibetan Plateau Research, Center for Excellence in Tibetan Plateau Earth Sciences, Chinese Academy of Sciences, Beijing 100101, China*

ABSTRACT

The present topography of the northern Tibetan Plateau is characterized by the northwest-trending Eastern Kunlun Range, Qaidam Basin, and Qilian Shan, which figure importantly into the evolution and mechanism of Tibetan plateau development during Cenozoic Indo-Asian convergence. Understanding the Cenozoic deformation history and the source-to-sink relationship through time has significant implications for deciphering the growth history of the northern Tibetan Plateau. Despite decades of study, the timing, pattern, and mechanisms of deformation across the northern Tibetan Plateau are still vigorously debated. The North Qaidam thrust belt, located between the Qaidam Basin and Qilian Shan thrust belt, provides a valuable record of Cenozoic deformation in the northern Tibetan Plateau. Here, we present the results of new geologic mapping, structural and sedimentology analysis, and apatite fission track thermochronology to constrain the Cenozoic evolution history and reconstruct the paleogeomorphology of the eastern domain of the North Qaidam thrust belt and its foreland, the Wulan Basin. Our analyses reveal the North Qaidam thrust belt experienced multi-phase exhumation since the Cretaceous. A period of Eocene localized thrust-related uplift of the North Qaidam thrust belt initiated shortly after India-Asia collision, and lower erosion rates in the Oligocene allowed the thrust belt to expand along-strike eastward. Local uplift shed sediments to the southwest, directly into the Qaidam Basin. Reactivation of the proximal thrust faults and initiation of the northwest-striking right-slip Elashan fault at ca. 15–10 Ma drove the final accelerated mid-Miocene cooling and denudation to the surface. This phase of deformation established the overall framework morphology of the northeastern margin of the Tibetan Plateau, including the overall structure of the basins and ranges.

[†]Corresponding authors: libing@cags.ac.cn; yongchao@cags.ac.cn.

INTRODUCTION

Understanding the spatiotemporal development of Cenozoic deformation across the Tibetan Plateau is critical in determining the mechanisms of crustal thickening and strain accommodation in continental tectonics (e.g., England and Houseman, 1986; Tapponnier et al., 1982, 2001; Yin et al., 2010; Zuza et al., 2020). Although the basic evolutionary history of the plateau has been established after decades of research, the distribution pattern, initial timing, and geodynamics of orogen-scale continental deformation remain debated (Meyer et al., 1998; Clark, 2012; Hough et al., 2011; Molnar et al., 1993, 2009; Royden et al., 2008; Tapponnier et al., 2001; Wang et al., 2008, 2014; Lin et al., 2016). Addressing the questions of when and how the Tibetan Plateau reached its modern elevation and established its northern margin can help us understand the processes of orogenic plateau construction (Burchfiel et al., 1991; Tapponnier et al., 2001; Wang et al., 2008; Yin, 2010; Clark, 2012; Wang et al., 2016a; Zuza et al., 2016).

The northeastern margin of the plateau is characterized by northwest-trending mountain ranges and basins, including the Eastern Kunlun Range, Qaidam Basin, and Qilian Shan (Shan = mountains in Chinese) from south to north, respectively (Fig. 1; Cheng et al., 2016a; Wu et al., 2019a). The Eastern Kunlun Range and Qilian Shan are active thrust belts, bounded by the active left-slip Altyn Tagh fault to the west, that accommodate largely distributed thrusting, crustal thickening, and complex strain partitioning during northward convergence (e.g., Zuza and Yin, 2016; Wu et al., 2019b; Cheng et al., 2021a). The left-slip Altyn Tagh fault has absorbed a large portion of thrusting and uplift across the whole present-day Qilian Shan (Meyer et al., 1998; Bovet et al., 2009; Zuza and Yin, 2016; Zhuang et al., 2018), and subordinately affected the interior of the Qaidam Basin by folding and reverse faulting (e.g., Chen et al., 2006; Wei et al., 2016; Wang et al., 2016b; Wu et al., 2019b). The Qaidam Basin represents a region of relatively lower strain between the aforementioned two deformation belts, and the North Qaidam thrust belt marking the transition between the Qaidam Basin and Qilian Shan (Fig. 1; Yin et al., 2008a, 2008b; Cheng et al., 2016a). The initiation timing and deformation pattern of the Cenozoic structures, and its role in impacting the deposition history of the related foreland basins, are poorly constrained.

There are broadly two end-member models for the Cenozoic growth and development of the northern Tibetan Plateau: (1) the in-sequence northeast-propagation model where deformation systematically propagated from the southern collisional zone of the Himalaya-Tibetan orogen to its northeast margin over the course of the Cenozoic (e.g., Meyer et al., 1998; Tapponnier et al., 2001; Zheng et al., 2010, 2017; Yu et al., 2019a, 2019b), with initial strain reaching the northeastern plateau in the middle Miocene or later (e.g., Yue and Liou, 1999; Meyer et al., 1998; Sun et al., 2005; Wang et al., 2020; Zheng et al., 2017; Pang et al., 2019); and (2) an out-of-sequence deformation model where growth of the northern Tibetan Plateau initiated

GSA Bulletin;
published online 12 May 2022
https://doi.org/10.1130/B36215.1; 11 figures; 1 supplemental file.

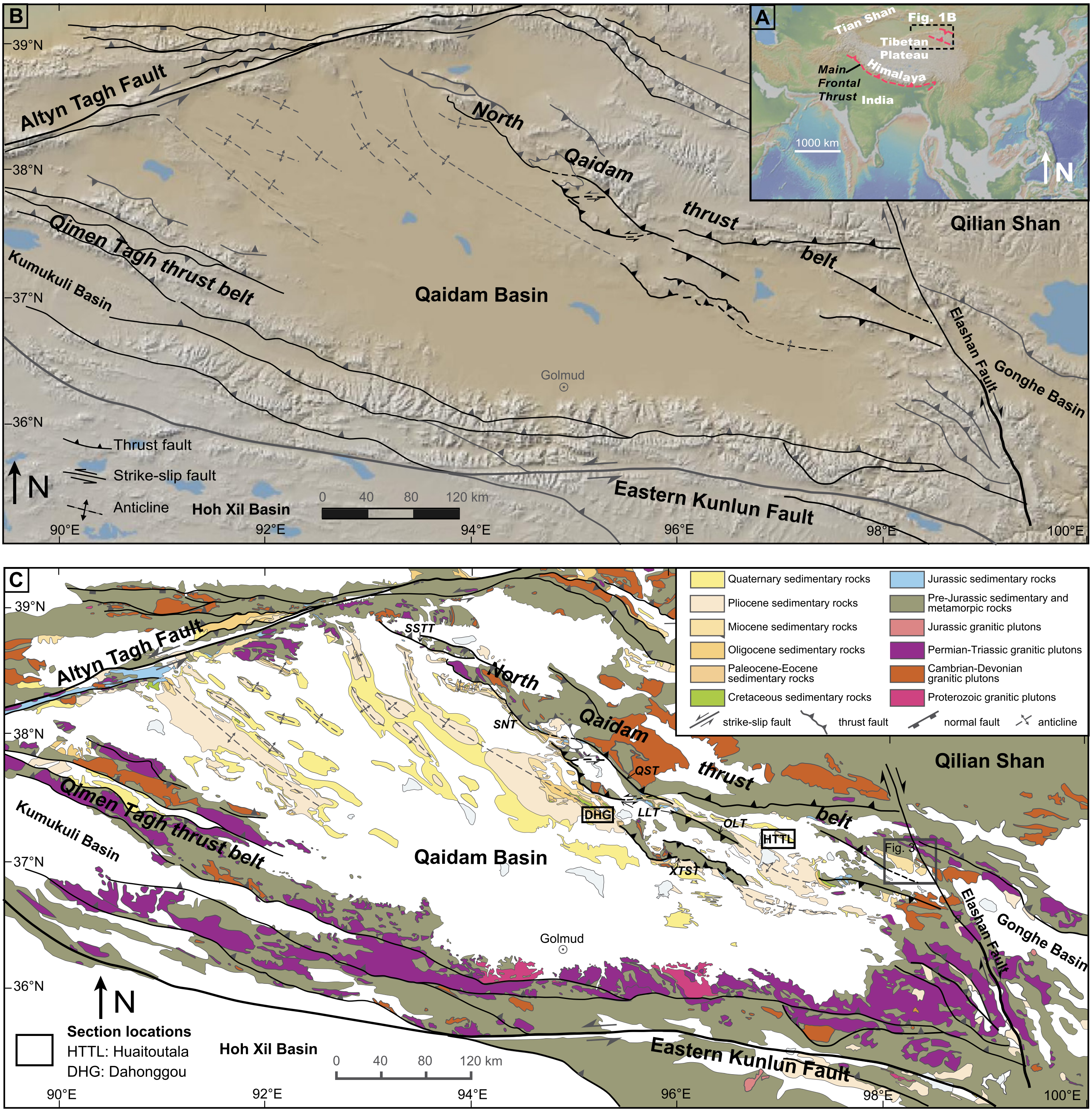

Figure 1. (A) Map of the Himalayan-Tibetan orogen showing the location of B as a dashed box. (B) Cenozoic tectonic map of the Qaidam Basin and surrounding area of the northern Tibetan Plateau. (C) Geologic map version of B (Yin et al., 2008a; Chen et al., 2012; Bush et al., 2016), showing the location of the previous published sections (see Fig. 2 for details), detailed geologic map of study area (see box labeled Fig. 3), and major thrust of the North Qaidam thrust belt. SSTT—Saishiteng thrust; SNT—Sainan thrust; QST—Qaidam Shan thrust; LLT—Luliang thrust; XTST—Xitie Shan thrust; OLT—Olongbulak thrust. Structures are from Yin et al. (2008a), Chen et al. (2012), Yu et al. (2017b), and Zuza et al. (2019). The digital topographic basemaps are from the GeoMapApp program (www.geomapapp.org) (Ryan et al., 2009).

shortly after the initial India-Asia collision in the Paleogene, and this region has persisted as the stationary boundary of the entire Tibetan Plateau since (Jolivet et al., 2001; Dupont-Nivet et al., 2004; Clark et al., 2010; Duvall et al., 2011, 2013; Zhuang et al., 2011; Cheng et al., 2015; Qi et al., 2016; He et al., 2018; Zuza et al., 2019; Wu et al., 2019c, 2021; An et al., 2020; Li et al., 2020, 2021). These previous studies highlight our incomplete understanding of the Cenozoic deformation pattern and intra-plate basin evolution within the northern Tibetan Plateau. Continuous sediment accumulation in the Qaidam Basin may have recorded the onset of exhumation across the basin-bounding ranges and associated switch of sediment depositional settings and sources. In this study, we focused on examining the sedimentary record in the Qaidam Basin to decipher and reconstruct the topographic growth history of the North Qaidam thrust belt since the early Cenozoic.

To determine the Cenozoic spatial-temporal evolution history and characterize the nature of the basin and range relationships across the North Qaidam thrust belt, we systematically conducted geologic mapping, structural and sedimentology analysis, and apatite fission track (AFT) thermochronology. This study focused on the eastern domain of the North Qaidam thrust belt, where the exposure of Proterozoic to Paleozoic bedrock and Miocene sediments in range-bounded basins allow us to reconstruct the cooling and basin-infilling history of this region. Taken together, we document a complex history of overprinting thrust and strike-slip faulting, and reconstruct the geomorphic evolution of the North Qaidam thrust belt. We argue the North Qaidam thrust belt experienced multi-phase growth history of Eocene fault-related uplift shortly after the India-Asia collision, which was followed by eastward along-strike expansion of the thrust belt in the Oligocene. Middle Miocene regional deformation reactivated the proximal thrust faults and initiated the northwest-striking Elashan right-slip fault at ca. 15–10 Ma, which established the overall framework morphology of the northeastern margin of the Tibet Plateau, including the overall structure of the basins and ranges.

GEOLOGIC SETTING

The >500-km-long North Qaidam thrust belt is located between the Qilian Shan to the north and Qaidam Basin to the south along the northern Tibetan Plateau. This NW-trending tectonic belt is geometrically truncated by the Altyn Tagh fault to the west and Elashan fault to the east (Fig. 1). The North Qaidam thrust belt consists of major contractional structures, including the Saishiteng thrusts, Sainan thrust, Qaidam Shan thrust, Luliang thrusts, Xitie Shan thrusts, Olongbulak thrust, and Aimunik thrust from west to east (Fig. 1C; Yin et al., 2008a). The south-directed thrust belt experienced a complex tectonic evolution through the Phanerozoic, associated with the early Paleozoic Qilian orogen (e.g., Yang et al., 2002; Song et al., 2013; Zuza et al., 2018), late Paleozoic Zongwulong orogen (e.g., Guo et al., 2009), Mesozoic evolution with early extension transitioning to compression in the Early Cretaceous (Chen et al., 2003; Wu et al., 2011; Yu et al., 2017a; Zhang et al., 2020), and Cenozoic contractional and transpressional deformation (e.g., Yin et al., 2008a, 2008b; Cheng et al., 2016a). The overprinting Cenozoic deformation juxtaposes Neoproterozoic gneisses, early Paleozoic ultrahigh-pressure metamorphic rocks, metamorphosed Ordovician-Silurian arc sequences, and Jurassic sedimentary rocks over the Cenozoic strata (Fig. 1C; e.g., Yang et al., 2001; Zhang et al., 2005; Yin et al., 2008a). The Cenozoic contractional structures resulting from the brittle deformation evolved consistently throughout the unmetamorphosed Devonian to Cenozoic strata, which differ from the development of ductile deformation in the pre-Devonian structures (Yang et al., 2001; Yin et al., 2008a).

The Cenozoic North Qaidam thrust belt is characterized by folds and thrust faults that accommodate the India-Asia convergence (e.g., Yin et al., 2008a, 2008b; Cheng et al., 2016a; Zuza et al., 2019). Cenozoic deformation and crustal shortening across the North Qaidam thrust belt are kinematically associated with the Qaidam Basin and the Qilian Shan thrust belt (Yin et al., 2007, 2008a, 2008b; Chen et al., 2010; Gao et al., 2013; Zuza et al., 2016). Below, we briefly describe the Cenozoic deformation of these two tectonic units.

Cenozoic Qaidam Basin

The Cenozoic Qaidam Basin, currently the largest interior depression inside the Tibetan Plateau, is surrounded by the Qilian Shan, the Eastern Kunlun Range, and the Altyn Tagh Range (Fig. 1B; e.g., Yin et al., 2002; Rieser et al., 2005; Chen et al., 2011; Cheng et al., 2016a; Wang et al., 2017). The overall present-day structure of the Cenozoic Qaidam Basin is dominated by a series of anticlines bounded by active thrust faults in the north and south that initiated at ca. 50 Ma and 30–20 Ma, respectively (Fig. 1C; Yin et al., 2008b), in response to the ongoing contractional strain generated by the India-Asia collision (Yin et al., 2008a; Chen et al., 2010). Growth strata from seismic interpretations indicates that Cenozoic deformation of the northern Qaidam Basin transitioned eastward since the early Eocene time (Yin et al., 2008a; Chen et al., 2010; Cheng et al., 2019a, 2021b), based on debated Cenozoic sediment age models outlined below.

The Cenozoic stratigraphy and their age estimates of the Qaidam Basin was recognized by detailed sedimentology, magnetostratigraphy, and various data sources (e.g., Yang et al., 1992; Xia et al., 2001; Sun et al., 2005; Rieser et al., 2006; Fang et al., 2007; Yin et al., 2008b; Chen et al., 2011; Cheng et al., 2016a; Bush et al., 2016; Ji et al., 2017; Wang et al., 2017; McRivette et al., 2019). Continuous Cenozoic sedimentary sequences are mainly composed of: (1) Lulehe Formation, Paleocene to early Eocene (ca. 53.5–43.8 Ma; Yang et al., 1992; Rieser et al., 2006; Ke et al., 2013; Yu et al., 2014a; Ji et al., 2017); (2) Xiaganchaigou Formation, middle Eocene to early Oligocene (43.8–35.5 Ma; Yang et al., 1992; Sun et al., 2005; Yu et al., 2014a; Li et al., 2016; Ji et al., 2017); (3) Shangganchaigou Formation, late Oligocene (35.5–22.0 Ma; Sun et al., 1999; Yu et al., 2014a; Chang et al., 2015; Li et al., 2016; Ji et al., 2017); (4) Xiayoushashan Formation, lower to middle Miocene (22.0–15.3 Ma; Sun et al., 1999; Chang et al., 2015; Li et al., 2016; Ji et al., 2017); (5) Shangyoushashan Formation, middle to late Miocene (15.3–8.2 Ma; Sun et al., 1999; Wang et al., 2007; Fang et al., 2007; Chang et al., 2015; Li et al., 2016; Ji et al., 2017); and (6) Shizigou Formation; upper Miocene and Pliocene (8.2–2.5 Ma; Sun et al., 1999; Fang et al., 2007; Wang et al., 2007; Yu et al., 2014a; Li et al., 2016; Fig. 2).

The Lulehe Formation, as the Cenozoic basal sedimentation in the Qaidam Basin, presumably represents the initiation of thrust-induced loading around the basin's periphery in response to the India-Asia convergence. However, the depositional age of the Lulehe Formation is highly debated, and two end-member age models have been proposed. The Lulehe Formation is generally considered to be Paleocene to early Eocene in age, based on previous magnetostratigraphy studies, regional lithostratigraphic correlations, spore and pollen assemblages, as well as seismic reflection interpretations (Yang et al., 1992; Rieser et al., 2006; Yin et al., 2008b; Ke et al., 2013; Ji et al., 2017; Cheng et al., 2019a, 2021b), but a recent age model proposes an Oligocene initial depositional age (ca. 30 Ma) of the Lulehe Formation, on the basis of the magnetostratigraphy study of the Dahonggou section in the northern Qaidam Basin (Fig. 1C; Wang et al., 2017). A younger Oligocene age for the Lulehe Formation would shift the overall age of Cenozoic sediments in the Qaidam Basin, and shift the timing of the deformation implied by the erosion and deposition of this detritus to be younger.

Cenozoic Qilian Shan Thrust Belt

The ~350-km-wide Cenozoic Qilian Shan thrust belt defines the northeastern margin of the Tibetan Plateau (Fig. 1B), which can be divided into the North Qilian Shan, Central Qilian Shan, and South Qilian Shan (e.g., Gehrels et al., 2003; Yue et al., 2005; Bovet et al., 2009; Yan et al., 2019). This tectonic belt is mainly comprised of

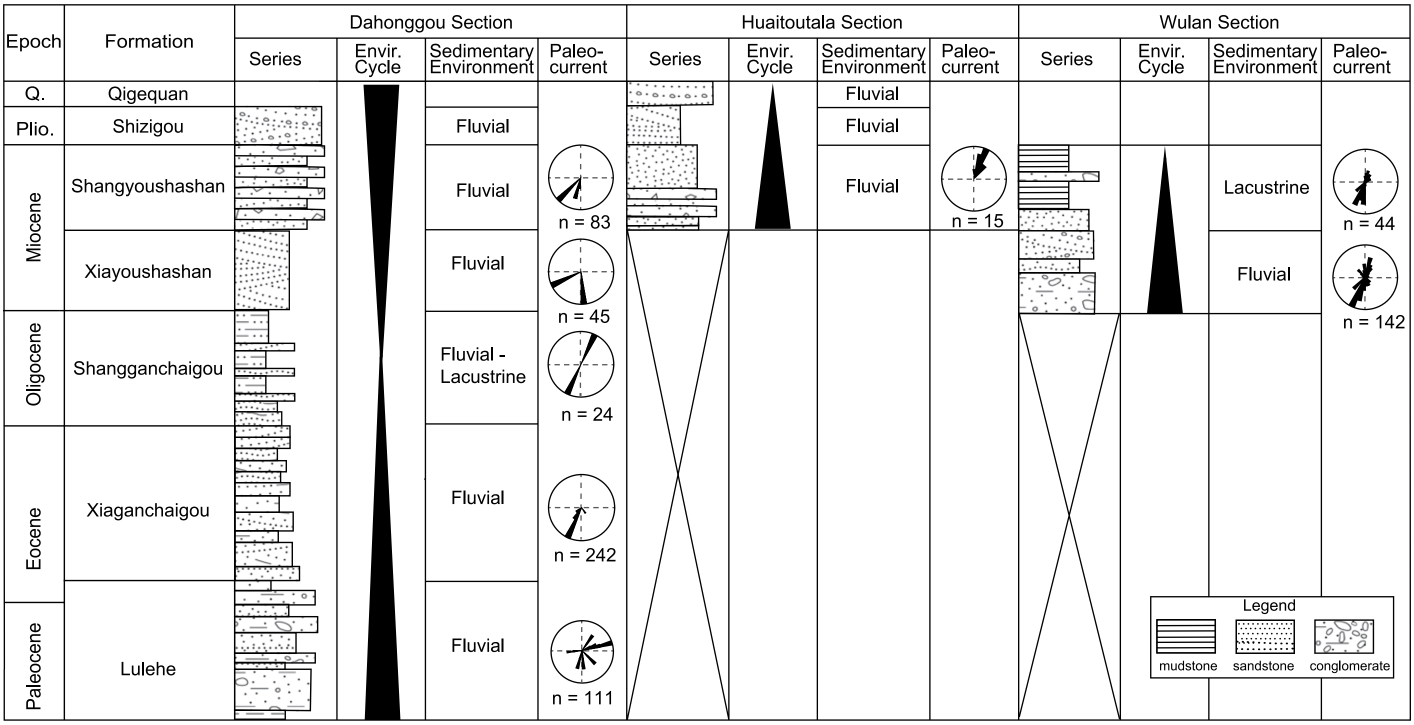

Figure 2. Generalized stratigraphic column of the Cenozoic series in the north Qaidam Basin, northern Tibetan Plateau. Lithology and sedimentary facies, and paleocurrent directions for the Dahonggou section were obtained from Lu and Xiong (2009) and Bush et al. (2016), whereas the sedimentary characteristics and paleocurrent data for the Huaitoutala section were obtained from Fang et al. (2007) and Pang et al. (2019), respectively. Deposit data for the Wulan section were measured in this study. The age ranges of each sequence are from Fang et al. (2007), Lu and Xiong. (2009), and Lu et al. (2012), respectively. Q.—Quaternary; Plio.—Pliocene; Envir. Cycle—Environment Cycle; n—number of paleo-current measurements.

NW-striking thrust and strike-slip faults overprinting the early frameworks originally formed during early Paleozoic orogeny and related arc-arc and arc-continent accretion (e.g., Song et al., 2013; Zuza et al., 2018; Li et al., 2021). The Qilian Shan thrust belt experienced widespread Jurassic–Cretaceous extension or transtension with the development of terrestrial basins (e.g., Vincent and Allen, 1999; Chen et al., 2003, 2004; Yin et al., 2008b; Zuza et al., 2018; He et al., 2019). This area also experienced a pulse of Early Cretaceous contractional deformation, triggered by far-field effects of the Lhasa-Qiangtang collision (Chen et al., 2019; Cheng et al., 2019c; He et al., 2019; Yu et al., 2019c; Zhang et al., 2020; Wang et al., 2021a).

Cenozoic deformation in the Qilian Shan generally involved mixed thrust and strike-slip faulting (Tapponnier et al., 2001; Duvall et al., 2013; Yuan et al., 2013; Yin et al., 2008a, 2008b; Zuza and Yin, 2016; Li et al., 2019, 2020). The Cenozoic strain appears to have propagated to the northern Tibetan Plateau by Eocene to Oligocene time (e.g., Jolivet et al., 2001; Clark et al., 2010; He et al., 2018; Cheng et al., 2016a; An et al., 2020; Li et al., 2020), and the exhumed Qilian Shan provided the clastic material deposited in both the Qaidam Basin to the south and Hexi Corridor to the north (Yin et al., 2008a; Bovet et al., 2009; Zhuang et al., 2011; Cheng et al., 2019b, 2019c; Yu et al., 2019c). Subsequent regional Miocene deformation across the Qilian Shan was accompanied by thrust-related rapid exhumation and the initiation of the major left-slip Haiyuan fault (e.g., Duvall et al., 2013; Yuan et al., 2013; Liu et al., 2019a; Zheng et al., 2017; Li et al., 2019, 2020; Yu et al., 2021a). Subsidiary right-slip faults, such as the Elashan and Riyueshan faults, initiated in the Miocene (Yuan et al., 2011; Cheng et al., 2021a) and are probably kinematically linked with the left-slip Haiyuan and Kunlun faults (e.g., Duvall and Clark, 2010; Cheng et al., 2021a). Therefore, protracted Cenozoic deformation has affected the region since the Eocene, and overprinted the complex pre-Cenozoic structures under the regime of the intracontinental strain accommodating the convergence of the India-Asia collision (e.g., Yin et al., 2008a, 2008b; Zuza et al., 2018, 2019; Chen et al., 2020; Li et al., 2021). Previous studies also show that tectonic activity in the Qilian Shan and the Qaidam Basin have been significantly enhanced during the Quaternary (Kapp et al., 2011; Yuan et al., 2011; Lu et al., 2015; Yu et al., 2015, 2021b; Bao et al., 2017; Liu et al., 2021).

STRUCTURAL GEOLOGY OF THE EASTERN DOMAIN OF NORTH QAIDAM THRUST BELT

The Cenozoic North Qaidam thrust belt bounds the southernmost part of the active Qilian Shan fold-thrust belt (Fig. 1B; Wang and Burchfiel, 2004; Yin et al., 2008a). The eastern domain of thrust belt, where this study was conducted, consists of the Buguote Shan, Wulan Basin, and Aimunik Shan from north to south, respectively (Figs. 1 and 3). Structures along the Buguote Shan trend northwest, which control the present-day morphology of the range. Cambrian-Ordovician metamorphic rocks are thrust over Miocene sediments by the Laohukou fault (f_2), which dips ~40–50° NE (Figs. 3 and 4A–4D; Site NQ1). Cambrian foliated marbles in fault zone display complex folds at Site NQ2 (Fig. 4E).

Southwest of field site NQ3 in our mapping area, the north-dipping thrust fault was directly observed in the field, which places Proterozoic metamorphic rocks over southward overturned Jurassic sandstone and continuous Cenozoic

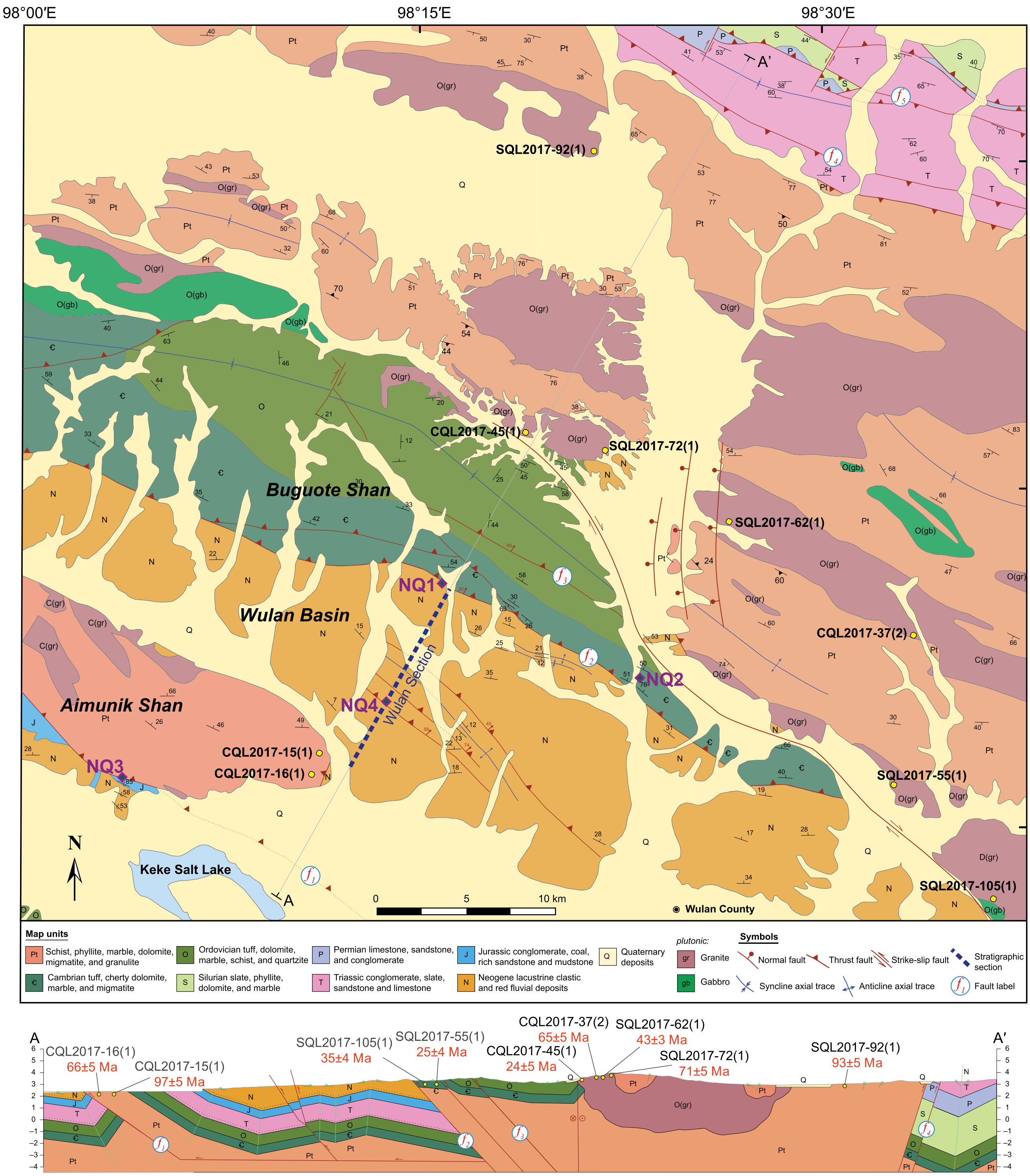

Figure 3. Geologic map (for location, see Fig. 1C) with sample locations (above), and cross section with apatite fission track ages of samples (below) across the easternmost segment of the North Qaidam thrust belt of the northern Tibetan Plateau based on Qinghai BGMR (1991) and our own detailed mapping. Annotations NQ1, NQ2, NQ3, and NQ4 correspond to field sites discussed in this study. f_1–Aimunik thrust; f_2–Laohukou Fault; f_3–Buguote Shan Fault; f_4–South Zongwulong Shan Fault; f_5–North Zongwulong Shan Fault; f_6–Elashan Fault.

sedimentary successions (Figs. 3, 5A, and 5B). Precise age constraints on these local Cenozoic sediments are lacking, but similar rocks have been inferred to be Miocene in the Wulan and nearby basins (Lu and Xiong, 2009; Lu et al., 2012). Lu et al. (2012) interpreted a set of dark red mudstone and conglomerate as the basal sediments of early Miocene age recorded within the Wulan basin. The presence of an unconfor-

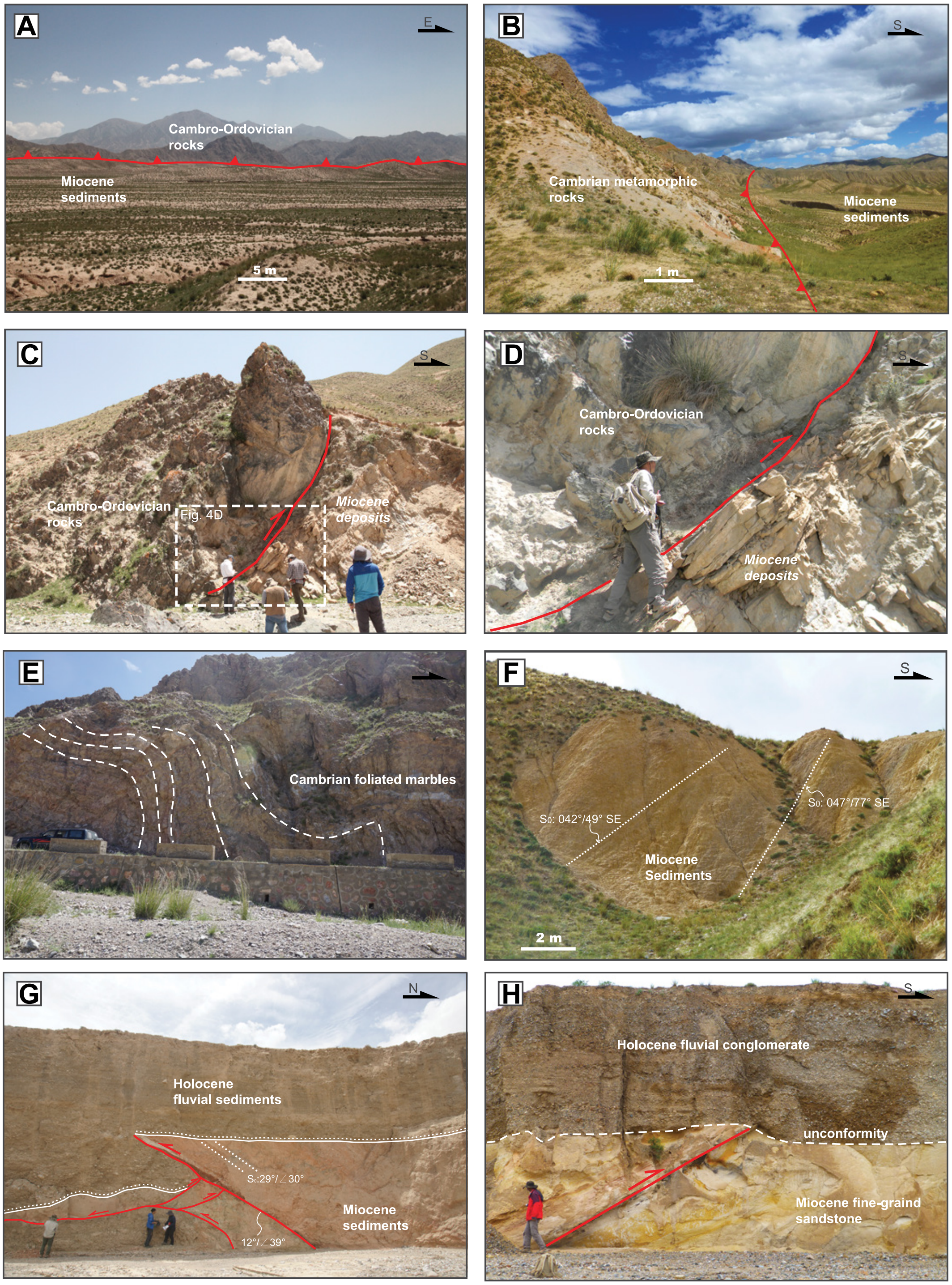

Figure 4. Field photographs of the easternmost segment of the North Qaidam thrust belt of the northern Tibetan Plateau highlighting important Miocene deformation relationships. (A–D) Views of the north-dipping Laohukou thrust fault (f_2), which places Cambro-Ordovician metamorphic rocks over gently north-dipping Miocene sediments (Fig. 3). This thrust system is the southern boundary of the Qilian Shan thrust belt, connecting to the east, along strike, with the Qinghai Nan Shan (e.g., Craddock et al., 2014). Photos were taken near site NQ1 (see Fig. 3). (E) View of the south vergent hanging-wall anticline in Cambrian thrust shown in A and B. Photo was taken at site NQ2. (F) Tilted Miocene strata developed in the Shangyoushashan Formation in the Wulan Basin, photo was taken near site NQ1. (G–H) North-dipping thrust fault with syn-tectonic Holocene basin-fill deposits. Photo was taken near site NQ4 (see Fig. 3). Note the attitudes reported in the figures are in the form of strike and dip.

mity between the early Miocene red mudstone and the underlying Jurassic coal-bearing strata could be observed in the field (Fig. 5A). The Miocene basal sediments and overlying yellowish brown sandstone were discordant by ~16° across tens of m (Fig. 5A), which we interpret to be resulting from the trishear deformation with the development of fault-related fold after the deposition of the early-Miocene sediments (e.g., Hardy and Ford, 1997; Allmendinger, 1998; Pei et al., 2017). These trishear-induced discordant relationships reflect pulses of Miocene deformation, which are commonly observed from seismic profiles across the Qaidam basin (e.g., Cheng et al., 2015; Pei et al., 2017).

The Wulan Basin is located in the northeastern most domain of the Qaidam Basin, and bounded by the Laohukou fault (f_2) to the north and the right-slip Elashan fault to the east, respectively (Fig. 3). Two continuous Miocene sedimentary successions of the Xiayoushashan Formation and Shangyoushashan Formation are well exposed within the basin, with age constraints from magnetostratigraphic data (Fang et al., 2007; Lu and Xiong, 2009; Lu et al., 2012). The most recent multi-phase thrusts crosscut the Miocene sediments, which are unconformably overlain by Holocene fluvial sediments in Site NQ4 (Figs. 4G and 4H). These faults dip ~40°–60° north, and

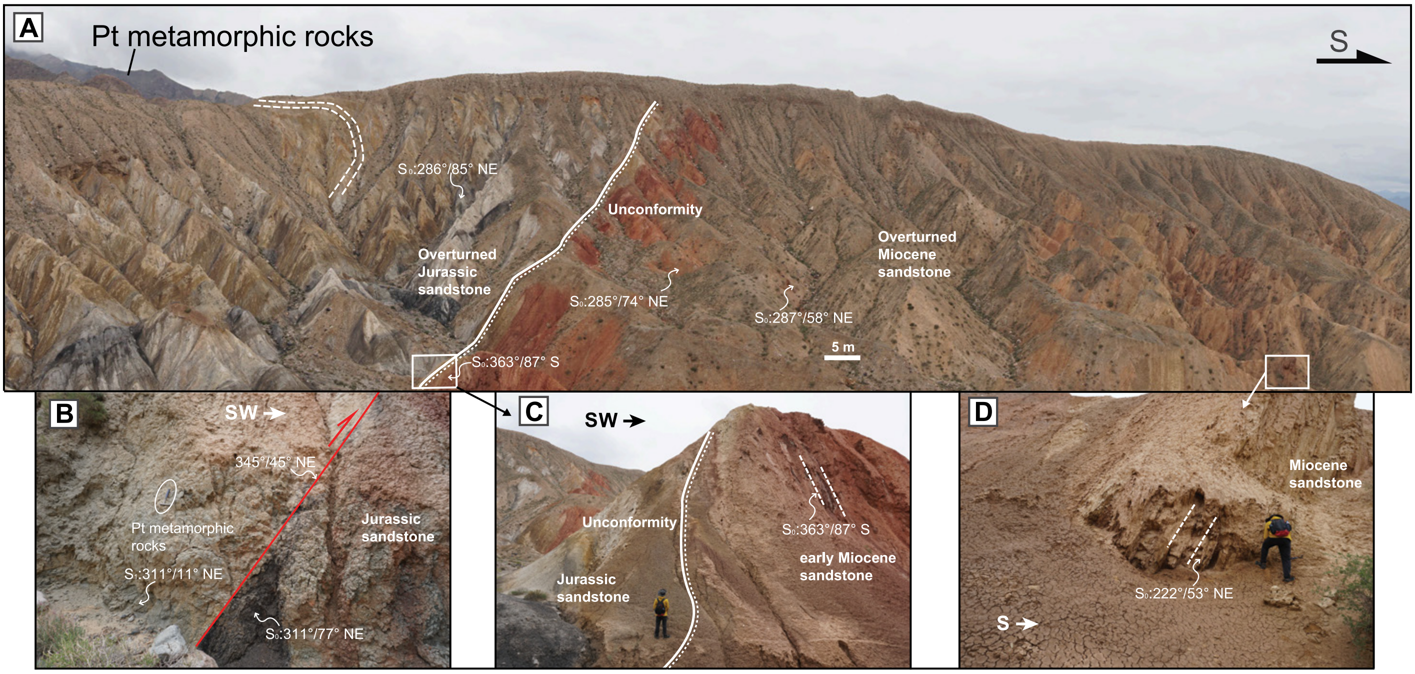

`Figure 5. Field photograph of the North Qaidam thrust belt of the northern Tibetan Plateau showing exposure of multi-phase deformation. The location of this site is NQ3 (see Fig. 3). (A) Interpreted field photograph of the overturned Jurassic and Cenozoic strata involved in mid-Miocene trishear thrusting as footwall anticline. (B) View of the north-dipping thrust fault, which places Proterozoic (Pt) metamorphic rocks over Jurassic coal-bearing sediments. (C–D) Field relations of the overturned Jurassic and Cenozoic strata with attitudes.

are parallel to the prominent range-bounding Laohukou fault (f_2) in map view (Fig. 3). This relationship indicates that the active thrusting propagated southward to the interior of the Wulan Basin along these newly formed faults, subsequently deforming footwall rocks of the thrust fault system.

STRATIGRAPHIC ANALYSIS IN WULAN BASIN

In order to characterize the stratigraphic architecture of the Wulan basin, we conducted a 2060 m field-based section and provenance analysis that spans the Cenozoic basin fill (Figs. 3, 6, and 7). Age constraints of the Wulan section are from magnetostratigraphic data of Lu et al. (2012). Provenance analysis was conducted in the Wulan section (nine sites) by measuring the paleocurrent orientations, which were determined from cross bedding and gravel imbrications. We recognized major depositional shifts based on facies distributions of the Xiayoushashan and Shangyoushashan formations (Fig. 7), which have assigned depositional ages of ca. 22–15 Ma and ca 15–8 Ma, respectively (Lu et al., 2012). This stratigraphic constraint could allow us to bracket the onset of deformation along the fault systems bounding the Wulan Basin, and reconstruct the tectonic paleogeomorphologic pattern of this region.

Xiayoushashan Formation

The 1025-m-thick Xiayoushashan Formation represents the initial deposit of the Wulan Basin, and is mainly comprised of coarse-grained fluvial and fine-grained lacustrine sediments. Dull-red deposits of the Xiayoushashan Formation (0–70 m) are distinctively characterized by normally graded, lenticular conglomerate, trough cross-stratified sandstone, and structureless to ripple siltstone and mudstone, with ~3–5 sedimentary cycles (Figs. 6A and 7A). Upper stratigraphic levels (70–390 m) include a set of regressively upward-fining sedimentary sequences. The lower part of the deposit is dominated by clast-supported, thick bedded or massive conglomerate containing clasts of 1–10 cm diameter, and intercalated with sandstone (Fig. 6B). The middle to upper part of this sequence commonly fines upward, and is characterized by coarse-grained sandstone of trough cross-bedding with interbedded siltstone and mudstone, to fine- to very fine-grained, ripple cross-stratified silty sandstone and mottled, 5–10-cm-thick beds of mudstone (Figs. 6C and 6D).

The intermediate succession (390–443 m) contains coarser material with few gravel clasts. The deposits consist of multistory glutenite bodies with sharp bases, these are composed of clast-supported, poorly sorted, granulecobble conglomerate interbedded with medium-to coarse-grained, horizontally and inclined stratified gravel sandstone (Fig. 6E). At 576–860 m, thick beds of coarse-grained, clast-supported, trough cross-stratified conglomerate are interbedded with fine- to very fine-grained, structureless siltstone. Above the fluvial deposits (860–1025 m), the frequency and thickness of sediments decrease, with deposits dominated by medium-fine grained, cross-stratified sandstone, ripple cross-stratified mudstone and clasts.

Lithofacies and strata geometries of the Xiayoushashan Formation are basically characteristic of two gravelly to sandy braided fluvial system (Fig. 7A). Coarse-grain size, cross-stratification, and lenticular bed geometries of the basal sediments are representative of proximal deposition in an aggradational channel belt. Paleocurrent directions measured for the Xiayoushashan Formation indicate variable southward flow (Fig. 7A), implying that transported clasts were derived from regions north of the Wulan Basin, most probably uplifted flanking ranges due to the early initiation of the North Qaidam thrust belt.

Shangyoushashan Formation

Compared to the sedimentary sequences of the Xiayoushashan Formation, the lithology of the 1035-m-thick Shangyoushashan Formation is relatively monotonous, and dominated by heavy-layered and mottled mudstone and

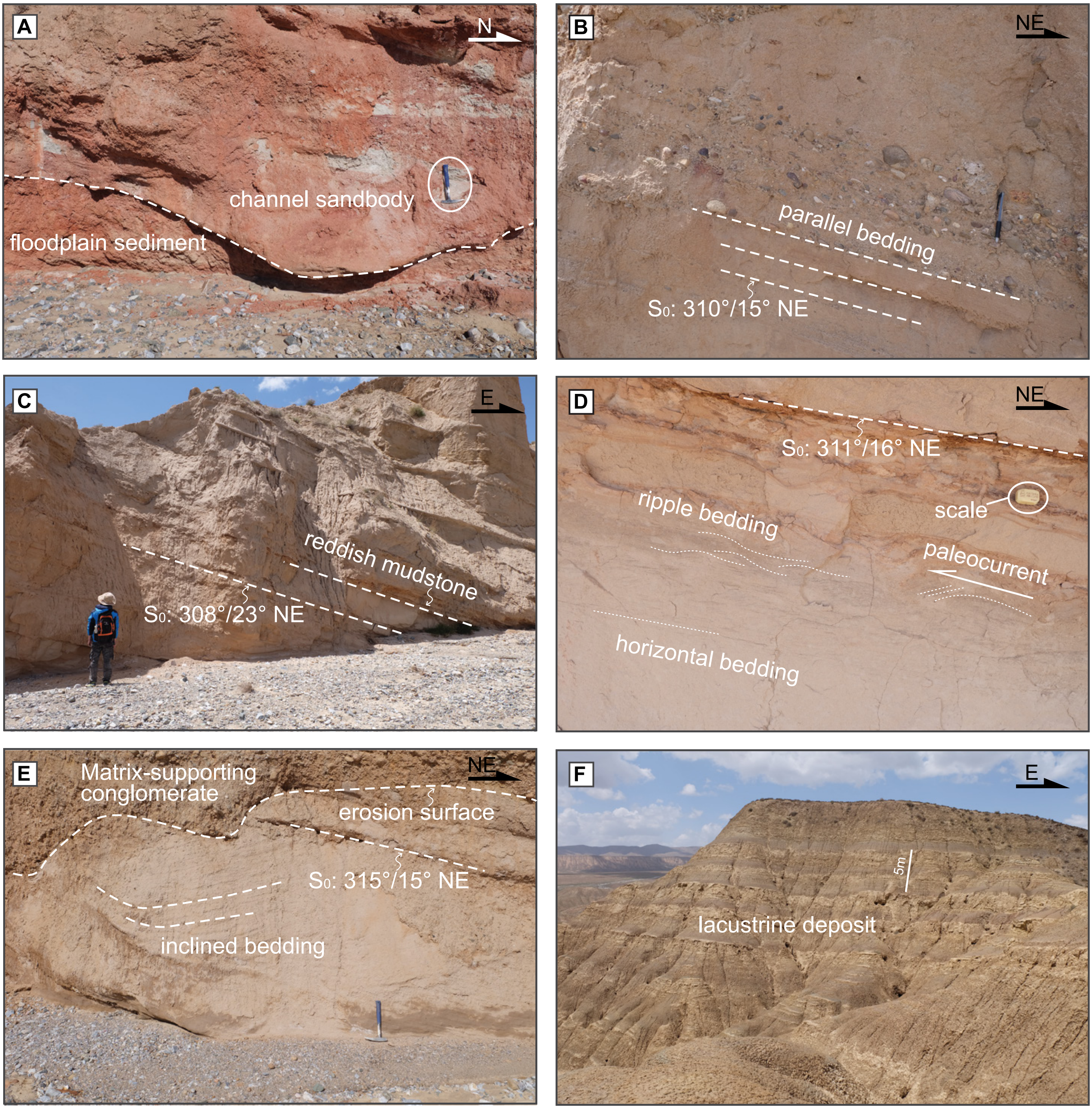

Figure 6. Typical field photographs of sedimentary characteristic in the Wulan Basin, northern Tibetan Plateau. (A) Lenticular sandstone deposited above the muddy overbank sediments, with widespread development of gray-greenish calcareous bands. (B) Horizontally stratified bedding of sandstone and conglomerate, indicating vertical aggradation of flatbed under high flow regime. (C) Tabular medium-grained sandstone interbedded with mudstone, suggesting shallow lacustrine environment. (D) Sandstone with horizontal bedding and ripple lamination developed in the shallow lacustrine environment. (E) Matrix-supported conglomerate interbedded with cross-stratified sandstone, indicating proximal rapid deposition. (F) Massive mudstone interbedded with thin-bedded silty sandstone, suggesting open lacustrine environment of the Shangyoushashan Formation. Note photos A–E were taken of the Xiayoushashan Formation.

laminated and fine-grained siltstone (Fig. 6F). This upward-thickening and upward-fining pattern in the Xiayoushashan Formation likely indicates a retrogradational system in which coarse-grained transverse fluvial systems regressed into the lacustrine systems. In addition, several sets of interbedded coarse-grained sediments of conglomerate and sandstone developed in this sequence, which could be interpreted as

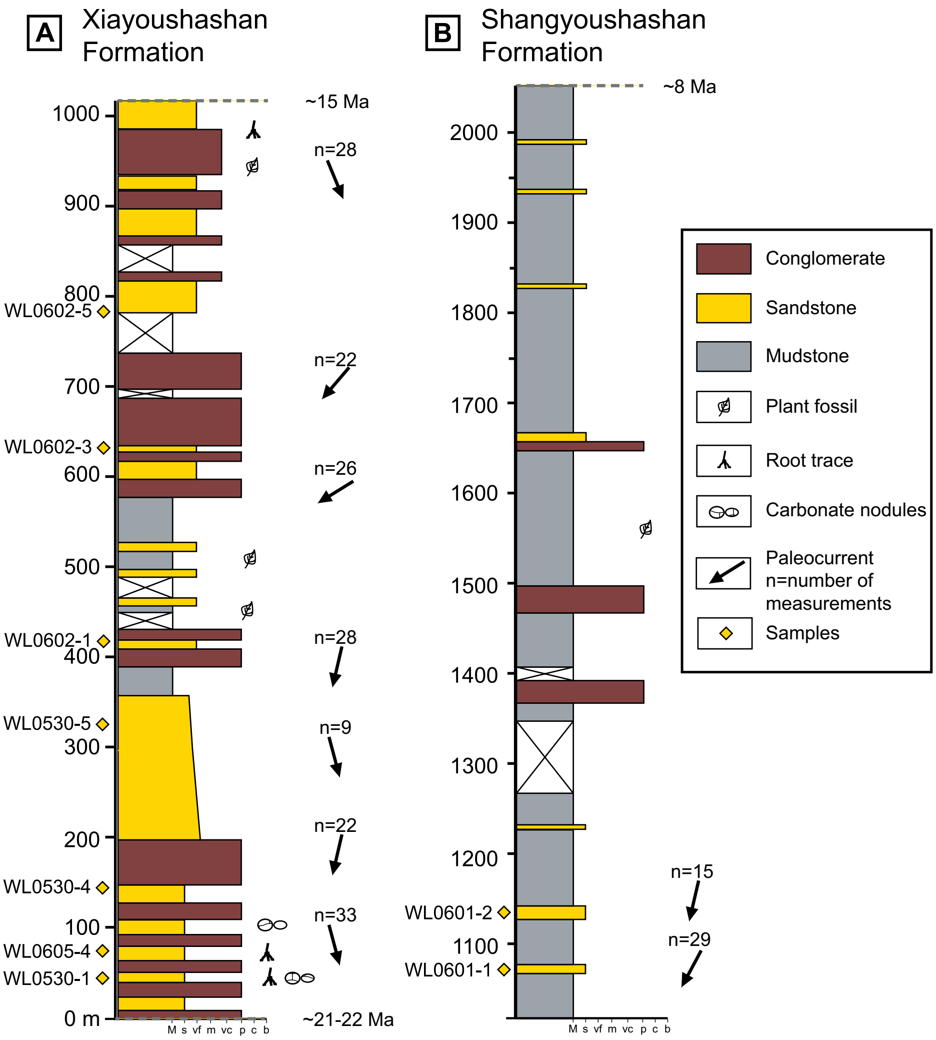

Figure 7. Stratigraphic columns for major depositional environments of the Wulan section in the northern Tibetan Plateau. Age assignment of the sediment units were from Lu et al. (2012). (A) Braided and meandering fluvial deposits of the early Miocene Xiayoushashan Formation. (B) Lacustrine deposits of the late Miocene Shangyoushashan Formation.

subaqueous turbid deposits (Fig. 7B). Paleocurrent directions measured for the Shangyoushashan Formation suggest apparent southeastward flow (Fig. 7B), indicating the transported detritus originated from the north and east regions of the north Qaidam and Elashan, respectively.

METHODS

Sandstone Petrology

Nine Miocene sandstone samples were collected from the Wulan Basin for petrographic analysis. We examined samples using a standard petrographic microscope to observe features such as the mineral composition, grain size, sorting, and roundness on standard and stained thin sections. Modal compositions were then measured with a minimum of 500 points using the modified Gazzi-Dickinson method on each thin section (Ingersoll et al., 1984). Detailed sample locations and raw point-counting data are summarized in the Table S1[1]. Samples were classified and plotted on the ternary diagrams using the scheme outlined in Dickinson et al. (1983). We follow the mineral abbreviation of Dickinson and Suczek (1979) to better describe our results: Qt—total quartz; Qm—monocrystalline quartz; F—feldspar; Lt—total lithic grains; Lv—volcanic lithic grains; and Ls—sedimentary lithic grains.

[1]Supplemental Material. Table S1: Detrital framework grain compositions of Miocene sandstones from the Wulan Basin, northern Tibetan Plateau. Table S2: Analytical data of the apatite fission track samples from the eastern domain of the North Qaidam thrust belt, northern Tibetan Plateau. Please visit https://doi.org/10.1130/GSAB.S.19372097 to access the supplemental material, and contact editing@geosociety.org with any questions.

Apatite Fission Track Thermochronology

We collected eight Neoproterozoic to Paleozoic granitoid samples and one sandstone sample for AFT analyses across the Cenozoic North Qaidam thrust belt. Apatite grains were separated using traditional heavy-liquid, magnetic, and handpicking separation techniques at the Hebei Institute of Geology and Mineral Resources in China. The apatite grains were then mounted in epoxy resin on glass slides, ground and polished to an optical finish to expose internal grain surface. Spontaneous tracks were revealed by 5.5% HNO_3 at 21 °C for 20 s. Thin low-uranium (<4 ppb) muscovite grains as external track detectors were packed together with apatite sample grain mounts and CN5 uranium glass dosimeters were irradiated in the well thermalized hot-neutron flux in the 492 Light-water reactor at China Institute of Atomic Energy, Beijing. Muscovite grains were detached and etched in 40% HF for 20 min at 25 °C to reveal the induced fission tracks (Yuan et al., 2003). Fission-track ages were measured and calculated at Beijing Zekang'en Technology Co. LTD in China by the zeta calibration approach (Hurford, 1990). Track densities for both natural and induced fission-track populations were measured with a dry objective magnification. Neutron fluence was monitored by CN5 uranium dosimeter glasses (Bellemans et al., 1995). The lengths of confined fission tracks and its corresponding the mean etch pit diameter (Dpar) values were measured by transmitted light microscopy with a Zeiss Axioplan 2. The zeta value is obtained by dating standard Durango and Fish Canyon Tuff apatite, with the value of 391 ± 17.8 a/cm^2. The Chi-square (χ^2) test was used to detect the probability of all analyzed age grains with the binomial "peak-fitting" method (Galbraith, 1990) by the RadialPlotter program (Vermeesch, 2009).

Thermal History Modeling

Considering the fission-track parameters and the particular geological setting of the northern Tibetan Plateau, we performed inverse modeling of the AFT data using the QTQt program of (v. 5.5.0; Gallagher, 2012) with the multi-kinetic annealing model of Ketcham et al. (2007) and Dpar values as a kinetic parameter. QTQt uses a Bayesian transdimensional Markov Chain Monte Carlo sampling method to generate a range of acceptable thermal histories, quantified in terms of a posterior probability distribution (Gallagher, 2012).

The inversion models were run with single grain ages and track lengths associated for each sample. The thermal history model inputs for simulations proceed from an initial randomly chosen time-temperature without any additional constrain to obtain the maximum interpolation range. Each inversion was run at 100,000 burn-in and 100,000 post-burn-in iterations, respectively, which are sufficient to provide stable models with their associated probabilities. This would allow the calculation of model statistics and the representative "expected" model (Gallagher, 2012). Samples were collected along a traverse across the east domain of the North Qaidam thrust belt, but most were not collected along a single vertical elevation profile (Fig. 3). Therefore, we modeled the AFT data for samples which passed the chi-square (χ^2) test individually. Based on the fission-track results (i.e., ages and lengths), the inversion modeling was performed with the following temperature constraints: (1) An initial condition began at high temperatures of 160–200 °C, as available AFT data indicated complete apatite annealing occurred at this high temperature. (2) The present-day surface temperature of 10 ± 10 °C by 0 Ma provided the final modeling constraint.

RESULTS

Sandstone Petrographic Results

Samples collected from the Wulan Basin are medium- to fine-grained sandstones, they are all well to moderately sorted and characterized by subangular to subrounded grains (Figs. 8A–8D). The average compositions of the lithics in the samples can reach up to 45.11% (Table S1; see footnote 1), although the lithic composition of single samples are relatively discrete. The overall transition pattern of samples in the QmFLt diagram shows good correspondence with their sedimentary process on the stratigraphic columns (Figs. 6 and 7).

Sample WL0530-1 is collected from the lower stratigraphic level of the Wulan section, and suggests a meandering river deposit system. The modal compositions of sample WL0530-1 are Qt: F: L = 44:11:45, Qm: F: Lt = 44:11:45, and Qp: Lv: Ls = 1:1:98, plotting into the "recycled orogen" field in the Qt-F-L and "quartzose recycled orogen" field in the Qm-F-Lt diagrams (Figs. 8E and 8F). Samples WL0530-4, WL0530-5, and WL0605-4 represent a retrogradational deposit system in which a coarse-grained braided river system regressed into the lacustrine system, and their average modal compositions are Qt:F:L = 64:10:26, Qm:F:Lt = 64:10:26, and Qp: Lv:Ls = 4:1:95, also plotting into the "recycled orogen" field in both the Qt-F-L and the "quartzose recycled orogen" field in the Qm-F-Lt diagrams (Figs. 8E and 8F).

Samples collected from the upper stratigraphic level of the Xiayoushashan Formation deposited in the fan-delta (WL0602-1) and braided river (WL0602-3 and WL0602-5) deposit systems showed average modal compositions of Qt: F: L = 53:10:37, Qm: F: Lt = 52:10:38, and Qp: Lv: Ls = 3:1:96, also plotting into the "recycled orogen" field in the Qt-F-L diagram. Samples WL0602-3 and WL0602-5 plotted in the "quartzose recycled orogen" field of the Qm-F-Lt diagram; whereas sample WL0602-1 plotted on the border of the "transitional recycled orogen" (Figs. 8E and 8F).

Sandstone samples WL0601-1 and WL0601-2 from the Shangyoushashan Formation indicated the subaqueous turbid current sediment system. The modal compositions of sample WL0601-1 are Qt: F: L = 30:7:63, Qm: F: Lt = 30:7:63, and Qp: Lv: Ls = 1:0:99, plotting into the magmatic field of the "undissected arc" in the Qt-F-L diagram and the "lithic recycled" field in the Qm-F-Lt diagram; whereas the modal compositions of sample WL0601-2 are Qt:F:L = 30:28:42, Qm:F:Lt = 29:28:42, and Qp:Lv:Ls = 1:0:99, plotting into the magmatic field of the "dissected arc" in the Qt-F-L and the Qm-F-Lt diagrams (Figs. 8E and 8F).

In the Qp-Lv-Ls diagram and the raw point-counting data (Table S1; see footnote 1), sedimentary lithic grains are the dominant composition of the total lithic fragments, which plot in the "collision orogen and fold-thrust belt" field of Figure 8G. The apparent increase of feldspar grains in sample WL0601-29 (Fig. 8F) may be related to the large-scale exhumation of the plutons from the Qilian orogen (e.g., Liu et al., 2019b; Li et al., 2021) and Zongwulong orogen (e.g., Guo et al., 2009) in the north. The clastic

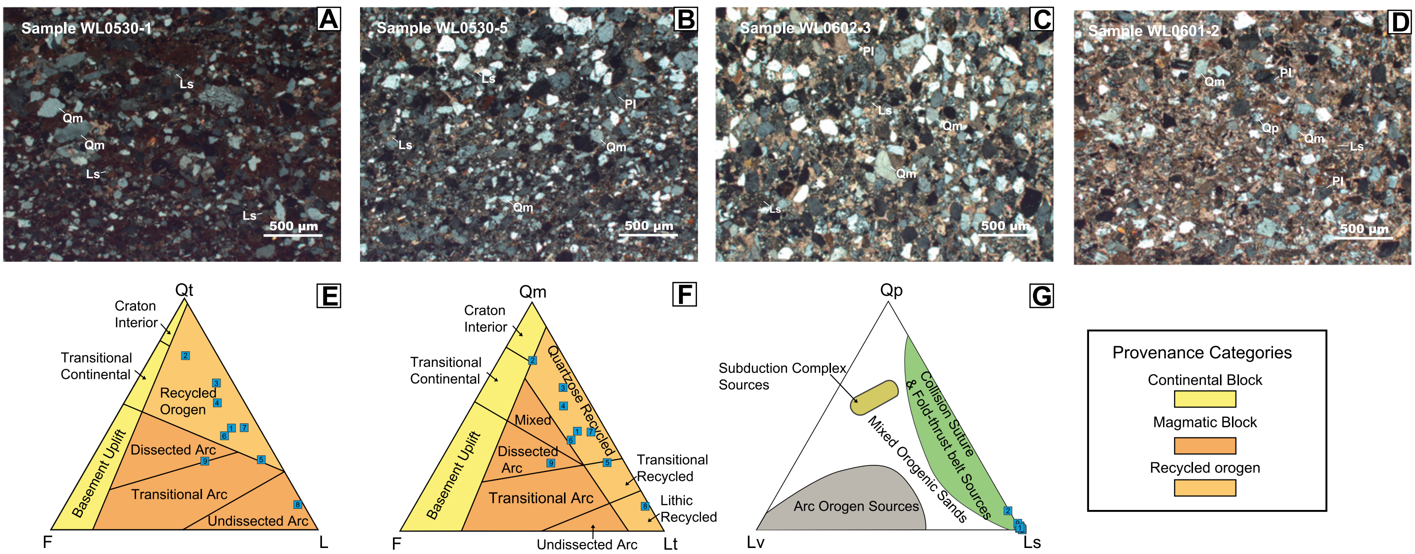

Figure 8. (A–D) Cross-polarized light photomicrograph of four representative Miocene samples from the Wulan Basin, northern Tibetan Plateau. (E–G) Ternary diagrams showing the relative abundance of framework grains in sandstone from the Miocene strata in the Wulan Basin. The provenance fields follow the method of Gazzi-Dickinson (Dickinson et al., 1983). Qt—total quartz; Qm—monocrystalline quartz; Qp—polycrystalline quartz; F—feldspar; L—lithic rock fragments; Lv—volcanic lithic fragments; Ls—sedimentaric lithic fragments; Lt—total lithic fragments (lithic rock fragments and polycrystalline quartz).

components of the sandstones in the Wulan Basin correspond with their sedimentary process, indicating the provenance distributions may be impacted by the multi-phase tectonic activities of the North Qaidam thrust belt.

Apatite Fission Track Results

Results obtained from AFT analysis of bedrock samples are listed in Table S2, including AFT ages, mean track lengths, and Dpar information. The AFT ages from nine bedrock samples can be divided into two distinct groups of Cretaceous and Cenozoic ages, ranging from 97 ± 5 Ma (1σ; Sample CQL2017-15(1)) to 24 ± 5 Ma (1σ; Sample CQL2017-45(1)). All AFT ages are much younger than their crystallization and depositional ages (Fig. 3; Guo et al., 2009), which represent the cooling ages that may record post-crystallization regional exhumation events. AFT ages for almost all analyzed samples passed the chi-square (χ^2) test (P (χ^2) < 5%; Galbraith, 1990) with the two exception of samples SQL2017-105(1) and CQL2017-16(1). The ratio plot of obtained single grain ages from this Devonian granite sample (SQL2017-105(1)) presents an age-dispersion of 64% and two dominated age populations of 67.2 ± 5.9 Ma (60.2 ± 8.6%) and 14.6 ± 1.3 Ma (39.8 ± 8.6%); whereas sample CQL2017-16(1) shows slight age-dispersion of 19% and two age peaks of 61.6 ± 3.9 Ma (79 ± 12%) and 103.0 ± 13.0 Ma (21 ± 12%) (Fig. 9; Vermeesch, 2009). The age dispersion

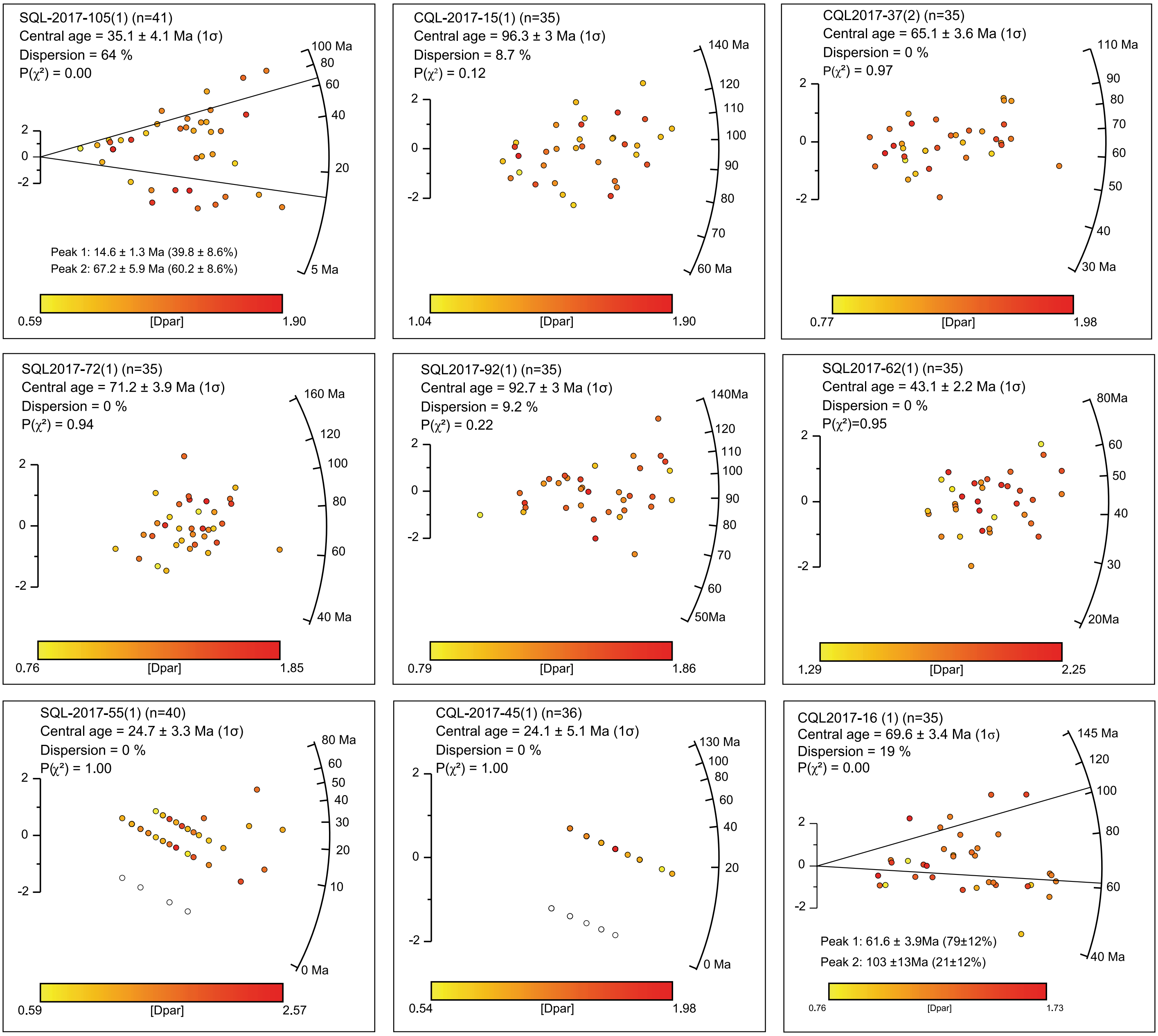

Figure 9. Apatite fission track radial plots (from RadialPlotter of Vermeesch, 2009) for bedrock samples from the eastern domain of the North Qaidam thrust belt, northern Tibetan Plateau with thermal history modeled. Single-grain ages are statistically split into two populations (Peak 1 and Peak 2) for samples SQL2017-105(1) and CQL2017-16(1) due to P (χ^2) < 5%.

could be attributed to the existing heavily annealed and shortened fission tracks causing difficulties in accurate identification of these tracks and/or a bias in the data acquisition (e.g., Gleadow et al., 1986; Green, 1988; Lin et al., 2011). For samples that passed the χ^2 test, the pooled ages are reported as AFT ages; otherwise, the central ages are adopted (Sobel et al., 2006).

In the analyzed apatite grains, mean track lengths range between 13.4 ± 1.9 μm and 10.4 ± 2.3 μm, with most proportion in the 12–13 μm range (Table S2). This suggests the track lengths in most of the samples have been shortened by annealing and indicates the samples have been experienced long-term annealing-related residence in the partial annealing zone (PAZ). Dpar values primarily range from 1.17 to 1.84 μm (Table S2).

Thermal History Modeling

The AFT cooling ages indicate when the mineral grain passed through the PAZ at 60–120 °C, which may not directly reflect a specific geological event given a complex tectonic and thermal history (Gleadow and Brown, 2000; Zhang and Wang, 2004; Flowers et al., 2015). Inverse thermal modeling is therefore required to infer the thermal history of samples (e.g., Ketcham et al., 2007; Gallagher, 2012). The AFT ages and measured track lengths can be inverted into thermal history models to reveal the cooling history of rocks within the shallow crust (e.g., Ketcham, 2005; Ketcham et al., 2007). In this work, two of nine samples were not modeled because not enough satisfactory mean track lengths were measured for modeling (Table S2; samples CQL2017-45(1) and SQL2017-55(1)).

In the thermal history modeling, sample SQL2017-92(1) reveals steady cooling from a temperature around the upper limit of the PAZ since the Early Cretaceous and residence in the PAZ until it was cooled rapidly through the lower limit of the PAZ since the Paleocene (Fig. 10). Samples CQL2017-37(2) and SQL2017-72(1) reflect steady cooling since the late Cretaceous (Fig. 10).

The time-temperature model for sample CQL2017-15(1) experienced Early Cretaceous cooling, subsequent long-term tectonic quiescence around the lower limit of the PAZ, and accelerated cooling to the surface since the Eocene (ca. 40 Ma); whereas sample SQL2017-105(1) underwent a long-term thermal stagnation within the PAZ since the Late Cretaceous, and a strong pulse of rapid cooling to the surface at mid-late Miocene time (ca. 10 Ma; Fig. 10).

DISCUSSION

Cenozoic Structural Deformation in the Eastern North Qaidam Thrust Belt

The field relationships presented in this study constrain the Mesozoic-Cenozoic kinematic history of the eastern North Qaidam thrust belt (Figs. 3–5). Previous field observations and seismic profile interpretation suggest that Paleozoic-Jurassic strata were subhorizontal across the northern Tibetan Plateau prior to the Cenozoic (Fig. 5; Zuza et al., 2018; Huang et al., 2021). There are observations across the northern Qaidam Basin and South Qilian Shan that suggest Early Cretaceous contractional deformation may have occurred locally (e.g., Cheng et al., 2019c, Zhang et al., 2020), but no significant late Paleozoic through Jurassic phases of deformation have been reported, and these strata regionally appear parallel (Fig. 3).

The Paleocene to early Eocene coarse-grained clastic deposit of the Lulehe Formation marks the initiation of the Cenozoic foreland sedimentation in the Qaidam Basin (Fig. 2; e.g., Yin et al., 2008b; Zhuang et al., 2011; Bush et al., 2016; Ji et al., 2017; Cheng et al., 2019a, 2021b; Wang et al., 2021b). However, one site in the northern Qaidam Basin has reinterpreted the Lulehe Formation age at Oligocene or Miocene (Wang et al., 2017; Nie et al., 2020). Here we prefer the Paleocene-Eocene assignment for the Lulehe Formation, which is based on independent studies across the Qaidam Basin (e.g., Yin et al., 2008b; Ji et al., 2017; Cheng et al., 2019a, 2021b), rather than a single site (Wang et al., 2017). Additional conformation of this older age model comes from flexural modeling of the Lulehe Formation that suggests there was a period of topographic load during its deposition induced by the rapid uplifting of the Qilian Shan (Cheng et al., 2018a; Wang et al., 2021b). Compiled thermochronology from the Qilian Shan shows pulses of exhumation throughout the Cenozoic (e.g., Ji et al., 2017; He et al., 2018; Li et al., 2020) and, therefore, the simplest model suggests that this Cenozoic exhumation loaded the Qaidam Basin and provided sediments for deposition in the early Cenozoic.

Based on the traditional age model for Cenozoic sediments in the Qaidam Basin, where the basal Lulehe Formation is Paleocene-Eocene (Fig. 2; e.g., Yin et al., 2008b; Cheng et al., 2019a), we interpret the early Cenozoic uplift in the North Qaidam thrust belt must have generated relief and erosion for the deposition of the Eocene strata in the Qaidam Basin and local Wulan Basin (Figs. 5; Yu et al., 2014a, 2017b). This may have been distal uplift, as the Eocene Xiaganchaigou Formation and Oligocene Shangganchaigou Formation growth-strata have been observed and interpreted across the nearby basins from seismic profiles and drilling data (Fig. 2; i.e., Yu et al., 2017b). In this study area, the Proterozoic metamorphic gneiss was thrust southwest over Jurassic sandstone and Cenozoic basin sediments (Figs. 5A and 5B). These early Miocene sediments were deposited unconformably with Jurassic strata, which might result from the Eocene-Oligocene deformation. Finally, a phase of Miocene-to-present south-directed faulting overturned the section to the south, which led to the development of the ~16° discordant within the Miocene sediments (Fig. 5A). This deformation continued to the present as evidenced by tilted strata within the Shangyoushashan Formation (Fig. 4D) and minor thrusts interior of the Wulan Basin cutting Miocene strata (Figs. 4G and 4H).

Late Cretaceous to Cenozoic Multi-Phase Cooling History of the North Qaidam Thrust Belt

Our new AFT ages and time-temperature thermal models suggest that the Neoproterozoic to Paleozoic rocks across the North Qaidam thrust belt were deeply buried and subsequently experienced multiple phases of cooling history and uplifting events through the Cretaceous to the present day.

The thermal histories for some samples suggest consistent slow cooling exhumation since Late Cretaceous to the present, and indicate that these samples have resided for a long-term period in the apatite PAZ through the Late Cretaceous to Cenozoic (Fig. 10). The rest of the samples yielded variable Cenozoic AFT ages and thermal histories (Table S2; Fig. 10). The inverse thermal histories for these samples suggest two broad Cenozoic cooling stages: pronounced cooling through the AFT PAZ in the early Eocene (ca. 40 Ma) and late Miocene (ca. 10 Ma; Fig. 10). The bimodal and complicated track-length distributions suggest phases of slight reheating, possibly due to thrust burial (Fig. 10).

In this case, bedrock samples with slow cooling exhumation since Late Cretaceous to the present revealed the progressive development of the northeastern Qaidam thrust belt (Fig. 10), which corresponds with the isostatic effects of the Cenozoic sedimentary accumulation in the Qaidam Basin (Yu et al., 2015; Yu and Guo. 2021); whereas multi-phase Cretaceous to present exhumations have also been observed across the eastern domain of the North Qaidam thrust belt. The first phase of the local Late Cretaceous cooling (Fig. 10), documented by our AFT results, suggests a period of regional exhumation, which corresponds with similar observations

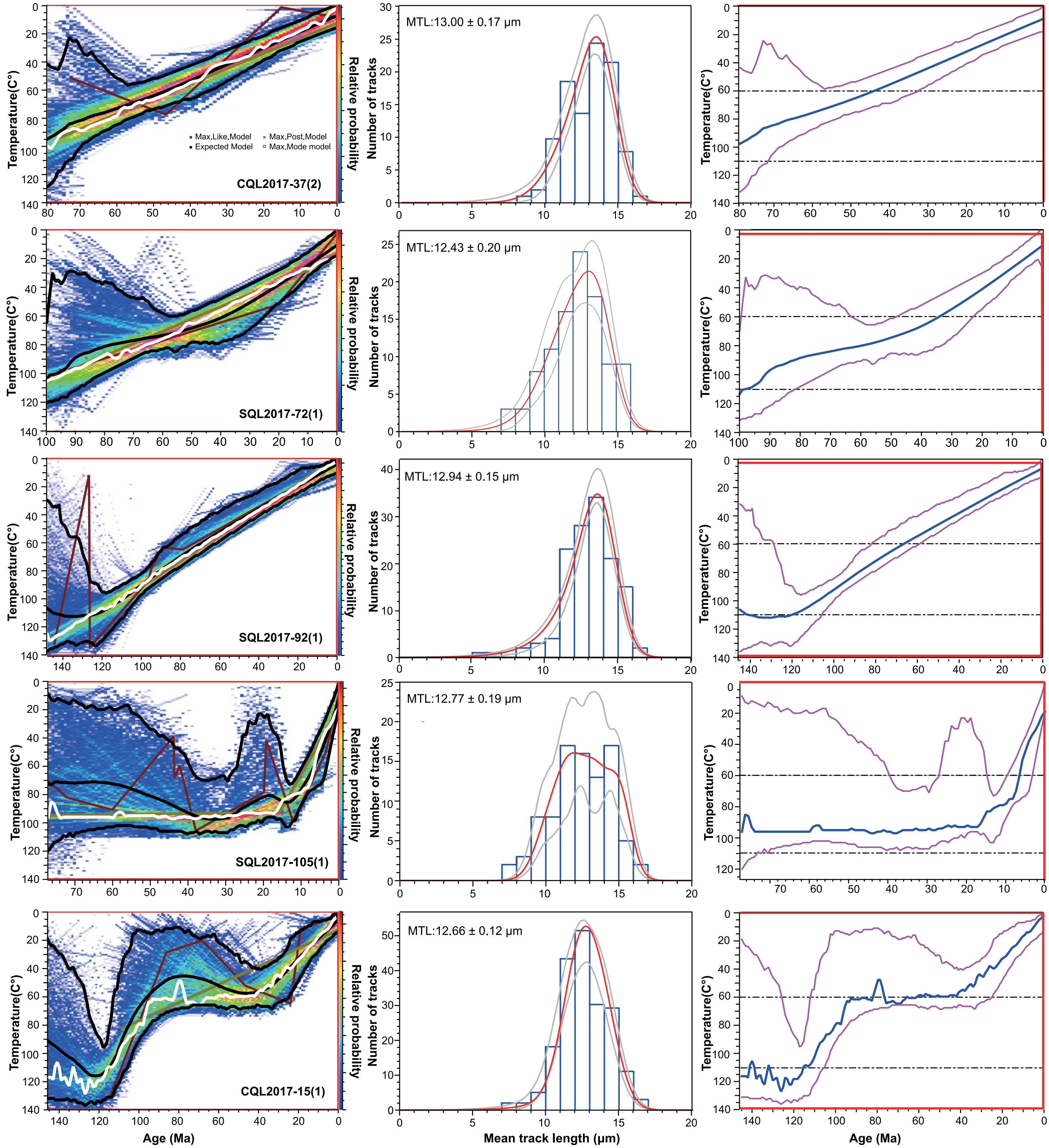

Figure 10. Apatite fission track thermal history models and length distributions of samples from the eastern domain of the North Qaidam thrust belt, northern Tibetan Plateau. The left and right plots display the thermal history models, in which the thick black lines show the expected model (i.e., average of all models weighted for their posterior probability); fine black lines indicate 95% credible intervals for the expected model; red box represents the prior time-temperature information. Middle hand plot displays the mean track length data that was inserted into the modeling program. More details can be found in Gallagher (2012).

elsewhere in the central segment of the North Qaidam thrust belt and the Qilian Shan to the north (Fig. 10; e.g., George et al., 2001; Cheng et al., 2016b; Yu et al., 2019a; Li et al., 2020). This phase of exhumation may have resulted in the Cretaceous exhumation of the Elashan Range (Jiang et al., 2008; Lu et al., 2012; Duvall et al., 2013), and the development of the Elashan highland (also referred to as the Dulan-Chaka highland; Duvall et al., 2013). The exact mechanism of this pulse of cooling has not been well constrained due to severe reactivation and overprinting by subsequent Cenozoic deformation, but it may possibly be due to the regional deformation driven by the far-field effects of the collision between the Lhasa and Qiangtang terranes during Middle Jurassic to Early Cretaceous (e.g., Kapp et al., 2007; Cheng et al., 2019c), which has been interpreted to have affected much of the northern Tibetan Plateau (e.g., Wu et al., 2011; Zhang et al., 2020; Wang et al., 2021a).

The period of rapid cooling since the Eocene, as revealed by sample CQL2017-15(1), may indicate the early initiation of the Aimunik thrust fault (f_1; Fig. 3) in response to the early Cenozoic collision of the India-Asia plates to the south (e.g., Hu et al., 2015; Zhu et al., 2015). This is also identified in the Qaidam Shan, Saishiteng Shan, and Zongwulong Shan from west to east across the North Qaidam thrust belt (Fig. 1C; Wang et al., 2004; Wan et al., 2011; Cheng et al., 2016b; Yu et al., 2017b). The existence of the unconformity between the Jurassic and Miocene strata is also evidence for early Cenozoic, pre-Miocene deformation (Fig. 5A). We propose that Eocene-Oligocene fault-related uplift led to local cooling, which shed the sediments to the southwest into the Qaidam Basin until at least early Miocene time. The Xiaganchaigou Formation had a small depocenter in the northeast Qaidam Basin that may have collected sediments shed from the study region (Yin et al., 2008b; Yu et al., 2014a; Cheng et al., 2018a).

The mid-late Miocene accelerated cooling corresponds to a widespread phase of exhumation across the North Qaidam thrust belt. Specifically, sample SQL 2017-105(1) from the fault-bounded area of North Qaidam thrust fault and right-slip Elashan fault (f_6) displays Miocene rapid cooling signal (Figs. 10). This phase of deformation led to south-directed thrusting and local overturning of Eocene-Miocene strata (Fig. 5A). Distributed Miocene growth strata have been observed throughout the Qaidam Basin based on field mapping and seismic profile interpretation (Fig. 4F; Cheng et al., 2016a, 2018b; 2021b; Yu et al., 2021a). These observations suggest widespread Miocene tectonic deformation along the thrust system and within the basin (Zhou et al., 2006;Yin et al., 2007, 2008a, 2008b; Wu et al., 2014; Cheng et al., 2016a, 2019c; Wei et al., 2016).

Structural and Sedimentary Evolution of the Eastern Qaidam Basin

We integrated field observations, sedimentologic analysis, thermochronology dating, and previous studies to reconstruct the tectonic evolution of the Wulan Basin. We identified variations in drainage patterns dictated by multi-episode shifts in the tectonic development of flanking the North Qaidam thrust belt and its related range growth. Results presented here document the Cenozoic depositional record in the Wulan Basin, and its relations to the northeastern Qaidam Basin and the broader northern Tibetan Plateau.

The Late Cretaceous contractional deformation and related range growth in the Elashan Range, recorded by previous studies and our AFT thermal history (i.e., samples SQL2017-72(1) and SQL2017-92(1)), indicate an early and constant exhumation of the Elashan fault (f_6). This could be interpreted as a northeastern onlap boundary of the Paleo-Wulan Basin, as the deposit of Cenozoic sediments north of the fault are negligible (Fig. 3). That said the Miocene strata would possibly pinch out in the depth of the Elashan fault (f_6; Fig. 3). The subsequent Eocene cooling signal from sample CQL2017-15(1) indicates the initiation of the Aimunik thrust fault (f_1) interior of the Paleo-Wulan Basin, which probably shed the deposits southwestward into the Qaidam Basin until the aforementioned early Miocene time (Yin et al., 2008b; Yu et al., 2014a; Cheng et al., 2018a).

In the Wulan Basin, the coarser-grained Xiayoushashan Formation (ca. 22–15 Ma), of conglomerate and sandstone, generally reflects braided river, braided river delta, and some of lacustrine sedimentary systems (Figs. 2 and 7A), suggesting the initial stages of basin development. Signs of soilification, such as gray-green calcareous bands, nodules, plant roots, and wormholes can be observed on the deposit sequence of the dull red, tens of meters thick, meandering sedimentary system of the lower stratigraphic level of the Xiayoushashan Formation (Fig. 7A). The extensive development of the early-mid Miocene high-energetic, braided river and delta deposits flowing southward indicate the Wulan Basin performed as a typical intermountain flexural basin and was mainly filled by the nearby Buguote Shan to the north and the Elashan Range to the east.

In the mid-late Miocene, the deposits in the Wulan Basin transitioned into a low-energy lacustrine sedimentary system of the Shangyoushashan Formation (ca. 15–8 Ma; Figs. 2 and 7B). However, the subaqueous turbid sediments of conglomerate and sandstone from our new measured stratigraphic section indicate the relief between the basin and range was still significant (Fig. 7B). This suggests the Wulan Basin was characterized with high water-level and underfilled lacustrine fan-delta system during the mid-late Miocene (e.g., Horton and Schmitt, 1996). This lacustrine fan-delta system, coupling with the high level of lithic fragments in the sandstones (Table S1, see footnote 1; Fig. 8) suggest the initiation of the Laohukou fault (f_2) and the right-slip Elashan fault (f_6), which bound the northern and eastern Wulan Basin (Figs. 1 and 3). The clastic components of the Miocene sandstones from the Wulan Basin also correspond with their depositional process (Fig. 8), indicating the provenance distributions may be impacted by the mid-Miocene thrust and strike-slip faulting of the eastern Qaidam Basin.

The Elashan Range, east of the Wulan Basin, may have experienced thrust-related protracted uplift since the Cretaceous to the early Oligocene as revealed by the AFT thermal history (Figs. 1 and 11A; Jiang et al., 2008; Lu et al., 2012; Duvall et al., 2013). This pre-Cenozoic existing Elashan highland led to the absence of Paleogene sediment in the surrounding region, and separated the eastern Qaidam Basin and western Gonghe Basin as independent sedimentary basins (Craddock et al., 2011; Lu et al., 2012). Previous studies have inferred the right-slip initial age of the Elashan fault at ca. 10–15 Ma based on estimated Quaternary slip rates at $\sim$1.1 mm/yr (Yuan et al., 2011; Cheng et al., 2021a) and apatite helium age from vertical transect (Duvall et al., 2013). Our study bolster the validity of this hypothesis based on the following observations and analysis: (1) the dominate rapid cooling signal from sample SQL2017-105(1) may also correspond to the lateral motion of the Elashan fault as the sample was collected from the footwall of the horsetail splay fault system (Fig. 3; Cheng et al., 2021a); (2) the retrogradational transition of the clastic provenance and the increasing of the lithic grains in the Miocene sandstones from the Wulan Basin indicate nearby exhumation of the Elashan Range, which was possibly associated with the slip motion of the Elashan fault (Figs. 8E and 11B; Table S1, see footnote 1). The synchronous uplift of the surrounding mountain ranges around the Wulan Basin led to the sedimentary system transition into a relatively topographically enclosed lacustrine environment (Fig. 11). On a larger scale, the deposits begin coarsening upward since the deposition of the Shangganchaigou Formation in the Dahonggou section (Fig. 1C). Fining sedimentation in the Huaitoutala section (Fig. 1C; Fang et al., 2007) and the Wulan section (this study) from west to

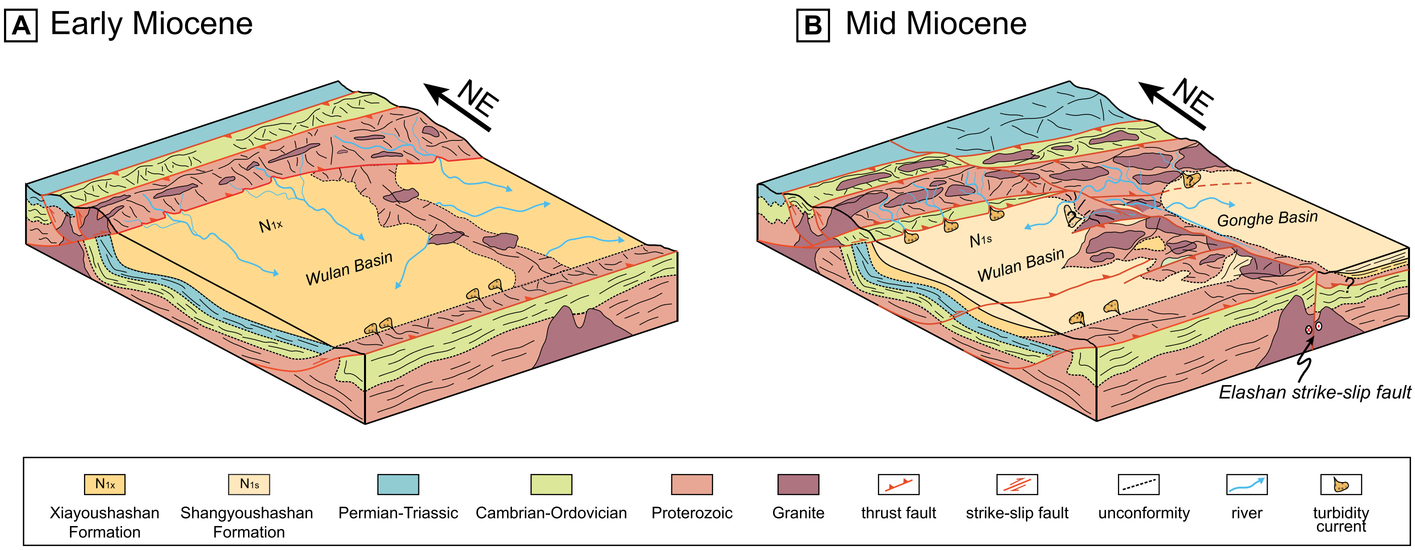

Figure 11. Late Cenozoic development and paleogeomorphic reconstruction in the east domain of the North Qaidam thrust belt, northern Tibetan Plateau (Modified from Wang et al., 2021c).

east, indicates the depocenter of the northern Qaidam Basin shifted eastward during the Miocene time (Fig. 2; Wang et al., 2006; Yin et al., 2007, 2008a; Chen et al., 2010; Yu et al., 2014a).

The northern Tibetan Plateau underwent a major pulse of regional mid-Miocene reorganization with the onset of the major left-slip faults (i.e., Haiyuan and Kunlun faults; e.g., Lease et al., 2011; Zuza and Yin, 2016; Cheng et al., 2018b; Wu et al., 2019c; Cheng et al., 2021a; Yu et al., 2021a). The subsidiary right-slip Elashan and Riyueshan faults may kinematically link to the left-slip faults related to left lateral extrusion (Tapponnier et al., 1982; Wang and Burchfiel, 2004; Cheng et al., 2015), and/or bookshelf faulting associated with clockwise fault rotation (England and Houseman, 1989; Zuza and Yin, 2016; Cheng et al., 2021a). Therefore, such widespread initiation of these intertwined strike-slip faults at ca. 15–10 Ma may have disrupted the previous sedimentary system and established the overall framework morphology across the northeast domain of the Qaidam Basin (Fig. 11; Craddock et al., 2011; Zhang et al., 2012; Cheng et al., 2021b and this study).

Cenozoic Expansion of the North Qaidam Thrust Belt during the Growth of the Northern Tibetan Plateau

Ascertaining the existence and exploring the mechanism of the early Cenozoic deformation in the northern Tibetan Plateau has significant implications for understanding the kinematics of intracontinental deformation of the Tibetan Plateau. This phase of contemporaneous early Cenozoic tectonic events has been supported by the published low temperature thermochronology ages across most of the northern Tibetan Plateau, such as in the Qimen Tagh, southern and northern margins of the Qaidam Basin, Qilian Shan, and western Qinling (e.g., Jolivet et al., 2001; Clark et al., 2010; Duvall et al., 2011; Zhuang et al., 2011, 2018; Cheng et al., 2016a, 2016b; Qi et al., 2016; Liu et al., 2017; He et al., 2018; Li et al., 2020). Specific to this study, observed Eocene AFT cooling and the apparent unconformity between the Jurassic and Miocene sediments (Figs. 5A and 10) suggest the North Qaidam thrust belt was exhuming in the early Cenozoic, implying the Cenozoic contractional strain transferred to the northern Tibetan Plateau shortly after the initial India-Asia collision at ca. 58 Ma (e.g., DeCelles et al., 2014; Hu et al., 2015, 2016).

Previous studies indicate that thrust-induced sedimentation in the Qaidam Basin began with the deposition of the Lulehe Formation (e.g., Ji et al., 2017; Cheng et al., 2018a; Wang et al., 2021b). The early Cenozoic sediments are relatively thin (i.e., <1000 m) and their distribution is restricted to the west-central part of the Qaidam Basin as revealed by the isopach maps (Yin et al., 2008b; Yu et al., 2014a; Cheng et al., 2018a). However, there is an apparent eastward expansion of sedimentation since the Oligocene time (e.g., Yu et al., 2014a) that we interpret may relate to deformation observed in field observations presented in Figure 5. The expansion of sedimentation in the Qaidam Basin may be triggered by the transition of the stress field (Yu et al., 2014a, 2014b) and/or the accelerated activity of the Altyn Tagh fault (e.g., Yin et al., 2002; Wu et al., 2012; Cheng et al., 2016a), where uplift of the Altyn Tagh Range blocked the westward flowing drainages and eventually closed off the contiguous interconnected Tarim-Qaidam Basin (Fig. 1C; Yin et al., 2002; Meng and Fang, 2008). With this interpretation, a closed Qaidam Basin (Yin et al., 2002; Yu and Guo, 2019) with a higher erosive base level, coupled with an overall dryer post-Eocene climate (e.g., Cheng et al., 2019b; Wu et al., 2021), could have dramatically reduced erosion rates in the growing basin-bounding mountain ranges. Less focused erosion promotes along-strike growth of the thrust belt (e.g., McQuarrie et al., 2008; Liu et al., 2020), in addition to promoting across-strike thrust belt expansion (e.g., Malavieille, 2010; Cheng et al., 2019b). Therefore, we interpret that expanded Oligocene to the present deposition in the Qaidam Basin reflects: (1) closure of the integrated Tarim-Qaidam Basin system shifting the Qaidam Basin depocenter eastward and (2) eastward growth of the North Qaidam thrust due to less focused erosion in the western part of the thrust belt (e.g., Hilley et al., 2004; Champagnac et al., 2012; Cheng et al., 2019b).

Our new obtained AFT thermochronology combined with previous data across the northern Tibetan Plateau indicate a period of accelerated mid-Miocene exhumation (e.g., (George et al., 2001; Jolivet et al., 2001; Craddock et al., 2011; Duvall et al., 2011; Yuan et al., 2013; Zheng et al., 2017; Zhuang et al., 2018; Li et al., 2019; Yu et al., 2019a, 2019b; Wang et al., 2020). This period of defamation is consistent with the initiation and development of the major strike-slip faults (e.g., Fu and Awata, 2007; Duvall et al., 2013; Yuan et al., 2013, Zuza and Yin, 2016; Li et al., 2019; Wu et al., 2019c; Yu et al., 2020), and may have resulted in the shift of deformation pattern from early thrusting to mixed-mode of thrust and strike-slip faulting (Lease et al., 2012; Yuan et al., 2013) in the middle Miocene time when the crustal thickening would have reached its present-day value (e.g., Zuza et al., 2020). This Miocene to the present pulse of deformation and synchronous range growth imply that contractional structures possibly having reactivated the older structures (e.g., Meyers et al., 1992; Zuza et al., 2018; Li et al., 2021), and established the current geomorphic and tectonic pattern of the northern Tibetan Plateau (e.g., Yuan et al., 2013).

CONCLUSIONS

Geologic mapping, field observations, sandstone petrologic and sedimentologic analysis, and AFT thermochronology dating provide constraints on the complex Cenozoic exhumation history, initiation ages of thrust and strike-slip faults, and the paleogeomorphic reconstruction of the North Qaidam thrust belt. The integrated results of our study have led to the following interpretations.

The North Qaidam thrust belt experienced uplift and exhumation in the Cretaceous due to a far-field tectonic response, Eocene-Oligocene thrust faulting and strata tilting, and the continued mid-Miocene to present exhumation.

Sandstone petrologic and sedimentologic results indicate the well-preserved Wulan Basin experienced a distinct two-stage evolution, with a switch from the fluvial stage to lacustrine stage during the mid-late Miocene. This transition may have been triggered by the growth of the surrounding ranges during the initiation of the right-slip Elashan fault at ca. 15–10 Ma.

Based on the previous studies and our observations, we argue the North Qaidam thrust belt experienced multiple phases of Cenozoic growth and expansion in response to the complex evolution of the northern Tibetan plateau. Eocene thrust-induced uplift and deformation may reflect an initial response to early Cenozoic India-Asia collision. The eastward Oligocene expansion of the North Qaidam thrust belt and related migration of the Qaidam Basin depocenter may be related to lower erosion rates induced by rising local base level and/or arid climate conditions in the Oligocene. Middle Miocene deformation that involved the initiation of major strike-slip fault systems established the current geomorphic tectonic pattern of the northern Tibetan Plateau.

ACKNOWLEDGMENTS

This research was jointly supported by the China Geological Survey (grants DD20221643 and D20190011), the National Natural Science Foundation of China (grants 42102261, 42022029, and 41874114), Chinese Academy of Geological Sciences (grant JKY21024), the National Key Research and Development Program of China (grant 2018YFC0603701), and the Tectonics Program of the National Science Foundation of the U.S. (grant EAR 1914501). Li gratefully thanks financial support from the China Scholarship Council (grant 201808110268) for funding his visit to the University of Nevada, Reno. Constructive reviews from Science Editor Wenjiao Xiao, Associated Editor Yongjiang Liu, Lei Wu, Xiangjiang Yu, and an anonymous reviewer are greatly appreciated and improved the presentation of our ideas. We thank Weicui Ding, Yiping Zhang, Yaoyao Zhang, Shenglin Xu, and He Su for assistance in the fieldwork and apatite fission track data analysis.

REFERENCES CITED

Allmendinger, R.W., 1998, Inverse and forward numerical modeling of trishear fault-propagation folds: Tectonics, v. 17, no. 4, p. 640–656, https://doi.org/10.1029/98TC01907.

An, K., Lin, X., Wu, L., Yang, R., Chen, H., Cheng, X., Xia, Q., Zheng, F., Ding, W., Gao, S., Li, C., and Zhang, Y., 2020, An immediate response to the Indian-Eurasian collision along the northeastern Tibetan Plateau: Evidence from apatite fission track analysis in the Kuantan Shan-Hei Shan: Tectonophysics, v. 774, https://doi.org/10.1016/j.tecto.2019.228278.

Bao, J., Wang, Y., Song, C., Feng, Y., Hu, C., Zhong, S., and Yang, J., 2017, Cenozoic sediment flux in the Qaidam Basin, northern Tibetan Plateau, and implications with regional tectonics and climate: Global and Planetary Change, v. 155, p. 56–69, https://doi.org/10.1016/j.gloplacha.2017.03.006.

Bellemans, F., De Corte, F., Den Haute, P.V., 1995, Composition of SRM and CN U-doped glasses: significance for their use as thermal neutron fluence monitors in fission track dating: Radiation Measurements, v. 24, p. 153–160, https://doi.org/10.1016/1350-4487(94)00100-F.

Bovet, P.M., Ritts, B.D., Gehrels, G., Abbink, A.O., Darby, B., and Hourigan, J., 2009, Evidence of Miocene crustal shortening in the north Qilian Shan from Cenozoic stratigraphy of the western Hexi Corridor, Gansu Province, China: American Journal of Science, v. 309, p. 290–329, https://doi.org/10.2475/00.4009.02.

Burchfiel, B.C., Zhang, P., Wang, Y., Zhang, W., Song, F., Deng, Q., Molnar, P., and Royden, L., 1991, Geology of the Haiyuan fault zone, Ningxia-Hui Autonomous Region, China, and its relation to the evolution of the northeastern margin of the Tibetan Plateau: Tectonics, v. 10, no. 6, p. 1091–1110, https://doi.org/10.1029/90TC02685.

Bush, M.A., Saylor, J.E., Horton, B.K., and Nie, J., 2016, Growth of the Qaidam Basin during Cenozoic exhumation in the northern Tibetan Plateau: Inferences from depositional patterns and multiproxy detrital provenance signatures: Lithosphere, v. 8, no. 1, p. 58–82, https://doi.org/10.1130/L449.1.

Champagnac, J.D., Molnar, P., Sue, C., and Herman, F., 2012, Tectonics, climate, and mountain topography: Journal of Geophysical Research. Solid Earth, v. 117, no. B2, https://doi.org/10.1029/2011JB008348.

Chang, H., Li, L.Y., Qiang, X.K., Garzione, C.N., Pullen, A., and An, Z.S., 2015, Magnetostratigraphy of Cenozoic deposits in the western Qaidam Basin and its implication for the surface uplift of the northeastern margin of the Tibetan Plateau: Earth and Planetary Science Letters, v. 430, p. 271–283, https://doi.org/10.1016/j.epsl.2015.08.029.

Chen, H.L., Yang, S.F., Xiao, A.C., Pan, Z.Z., Cheng, X.G., Chen, J.J., Fan, M.T., and Tian, D.W., 2006, Deformation characteristics and time of Cenozoic thrust belt in southern margin of Jiuquan basin [in Chinese with English abstract]: Oil & Gas Geology, v. 27, no. 4, p. 488–494.

Chen, L., Liu, L., Capitanio, F.A., Gerya, T.V., and Li, Y., 2020, The role of pre-existing weak zones in the formation of the Himalaya and Tibetan plateau: 3-D thermomechanical modelling: Geophysical Journal International, v. 221, no. 3, p. 1971–1983, https://doi.org/10.1093/gji/ggaa125.

Chen, X., Yin, A., Gehrels, G.E., Cowgill, E.S., Grove, M., Harrison, T.M., and Wang, X.-F., 2003, Two phases of Mesozoic north-south extension in the eastern Altyn Tagh range, northern Tibetan Plateau: Tectonics, v. 22, no. 5, https://doi.org/10.1029/2001TC001336.

Chen, X., Yin, A., Gehrels, G.E., Cowgill, E.S., Grove, M., Harrison, T.M., Wang, X.F., Yang, N., and Liu, J., 2004, Mesozoic N-S extension in the eastern Altyn Tagh range on the northern margin of the Qinghai-Tibet plateau [in Chinese with English Abstract]: Journal of Geomechanics, v. 10, no. 3, p. 193–212.

Chen, X.H., Dang, Y.Q., Yin, A., Wang, L.Q., Jiang, W.M., and Li, L., 2010, Basin mountain coupling and tectonic evolution of Qaidam Basin and its adjacent orogenic belts [in Chinese]. Beijing, China, Geological Publishing House, 365 p.

Chen, X.H., McRivette, M.W., Li, L., Yin, A., Jiang, R.B., Wan, J.L., and Li, H.J., 2011, Thermochronological evidence for multi-phase uplifting of the East Kunlun Mountains, northern Tibetan Plateau [in Chinese with English abstract]: Geological Bulletin of China, v. 30, no. 11, p. 1647–1660.

Chen, X.H., Gehrels, G.E., Yin, A., Li, L., and Jiang, R.B., 2012, Paleozoic and Mesozoic basement magmatisms of eastern Qaidam Basin, Northern Qinghai-Tibet Plateau: LA-ICP-MS zircon U-Pb geochronology and its geological significance: Acta Geologica Sinica, v. 86, p. 350–369, https://doi.org/10.1111/j.1755-6724.2012.00665.x.

Chen, X., Shao, Z., Xiong, X., Gao, R., Xu, S., Zhang, Y., Li, B., and Wang, Y., 2019, Early Cretaceous overthrusting of Yumu mountain and hydrocarbon prospect on the Northern margin of the Qilian orogenic belt [in Chinese with English abstract]: Acta Geoscientica Sinica, v. 40, no. 3, p. 377–392, https://doi.org/10.3975/cagsb.2019.050901.

Cheng, F., Jolivet, M., Dupont-Nivet, G., Wang, L., Yu, X., and Guo, Z., 2015, Lateral extrusion along the Altyn Tagh Fault, Qilian Shan (NE Tibet): Insight from a 3D crustal budget: Terra Nova, v. 27, no. 6, p. 416–425, https://doi.org/10.1111/ter.12173.

Cheng, F., Fu, S.T., Jolivet, M., Zhang, C.H., and Guo, Z.J., 2016a, Source to sink relation between the Eastern Kunlun Range and the Qaidam Basin, northern Tibetan Plateau, during the Cenozoic: Geological Society of America Bulletin, v. 128, no. 1–2, p. 258–283, https://doi.org/10.1130/B31260.1.

Cheng, F., Garzione, C., Jolivet, M., Guo, Z., Zhang, D., and Zhang, C., 2018a, A new sediment accumulation model of Cenozoic depositional ages from the Qaidam basin, Tibetan Plateau: Journal of Geophysical Research. Earth Surface, v. 123, p. 3101–3121, https://doi.org/10.1029/2018JF004645.

Cheng, F., Garzione, C.N., Jolivet, M., Guo, Z., Zhang, D., Zhang, C., and Zhang, Q., 2019a, Initial deformation of the northern Tibetan plateau: Insights from deposition of the Lulehe Formation in the Qaidam Basin: Tectonics, v. 38, no. 2, p. 741–766, https://doi.org/10.1029/2018TC005214.

Cheng, F., Garzione, C.N., Mitra, G., Jolivet, M., Guo, Z., Lu, H., Li, X., Zhang, B., Zhang, C., Zhang, H., and Wang, L., 2019b, The interplay between climate and tectonics during the upward and outward growth of the Qilian Shan orogenic wedge, northern Tibetan Plateau: Earth-Science Reviews, v. 198, https://doi.org/10.1016/j.earscirev.2019.102945.

Cheng, F., Jolivet, M., Guo, Z., Lu, H., Zhang, B., Li, X., Zhang, D., Zhang, C., Zhang, H., Wang, L., Wang, Z., and Zhang, Q., 2019c, Jurassic–Early Cenozoic tectonic inversion in the Qilian Shan and Qaidam Basin, North Tibet: New insight from seismic reflection, isopach mapping, and drill core data: Journal of Geophysical Research. Solid Earth, v. 124, no. 11, p. 12,077–12,098, https://doi.org/10.1029/2019JB018086.

Cheng, F., Zuza, A.V., Haproff, P.J., Wu, C., Neudorf, C., Chang, H., Li, X., and Li, B., 2021a, Accommodation of India-Asia convergence via strike-slip faulting and block rotation in the Qilian Shan fold-thrust belt, northern margin of the Tibetan Plateau: Journal of the Geological Society, v. 178, no. 3, https://doi.org/10.1144/jgs2020-207.

Cheng, F., Jolivet, M., Guo, Z., Wang, L., Zhang, C., and Li, X., 2021b, Cenozoic evolution of the Qaidam basin and implications for the growth of the northern Tibetan plateau: A review: Earth-Science Reviews, v. 220, https://doi.org/10.1016/j.earscirev.2021.103730.

Cheng, X., Lin, X., Wu, L., Chen, H., Xiao, A., Gong, J., Zhang, F., and Yang, S., 2016b, The exhumation history of North Qaidam thrust belt constrained by apatite fission track thermochronology: Implication for the evolution of the Tibetan Plateau [English edition]: Acta Geologica Sinica, v. 90, no. 3, p. 870–883, https://doi.org/10.1111/1755-6724.12730.

Cheng, X., Zhang, D., Jolivet, M., Yu, X., Du, W., Liu, R., and Guo, Z., 2018b, Cenozoic structural inversion from transtension to transpression in Yingxiong Range, western Qaidam Basin: New insights into strike-slip superimposition controlled by Altyn Tagh and Eastern Kunlun Faults: Tectonophysics, v. 723, p. 229–241, https://doi.org/10.1016/j.tecto.2017.12.019.

Clark, M.K., 2012, Continental collision slowing due to viscous mantle lithosphere rather than topography: Nature, v. 483, p. 74–77, https://doi.org/10.1038/nature10848.

Clark, M.K., Farley, K.A., Zheng, D., Wang, Z., and Duvall, A.R., 2010, Early Cenozoic faulting of the northern Tibetan Plateau margin from apatite (U-Th)/He ages: Earth and Planetary Science Letters, v. 296, no. 1–2, p. 78–88, https://doi.org/10.1016/j.epsl.2010.04.051.

Craddock, W., Kirby, E., and Zhang, H., 2011, Late Miocene–Pliocene range growth in the interior of the northeastern Tibetan Plateau: Lithosphere, v. 3, no. 6, p. 420–438, https://doi.org/10.1130/L159.1.

Craddock, W.H., Kirby, E., Zhang, H., Clark, M.K., Champagnac, J.D., and Yuan, D., 2014, Rates and style of Cenozoic deformation around the Gonghe Basin, northeastern Tibetan Plateau: Geosphere, v. 10, p. 1255–1282, https://doi.org/10.1130/GES01024.1.

DeCelles, P.G., Kapp, P., Gehrels, G.E., and Ding, L., 2014, Paleocene–Eocene foreland basin evolution in the Himalaya of southern Tibet and Nepal: Implications for the age of initial India-Asia collision: Tectonics, v. 33, no. 5, p. 824–849, https://doi.org/10.1002/2014TC003522.

Dickinson, W.R., and Suczek, C.A., 1979, Plate tectonics and sandstone compositions: AAPG Bulletin, v. 63, p. 2164–2182.

Dickinson, W.R., Beard, L.S., Brakenridge, G.R., Erjavec, J.L., Ferguson, R.C., Inman, K.F., Knepp, R.A., Lindberg, F.A., and Ryberg, P.T., 1983, Provenance of North American Phanerozoic sandstones in relation to tectonic setting: Geological Society of America Bulletin, v. 94, p. 222–235, https://doi.org/10.1130/0016-7606(1983)94<222:PONAPS>2.0.CO;2.

Dupont-Nivet, G., Horton, B.K., Butler, R.F., Wang, J., Zhou, J., and Waanders, G.L., 2004, Paleogene clockwise tectonic rotation of the Xining-Lanzhou region, northeastern Tibetan Plateau: Journal of Geophysical Research. Solid Earth, v. 109, no. B4, https://doi.org/10.1029/2003JB002620.

Duvall, A.R., and Clark, M.K., 2010, Dissipation of fast strike-slip faulting within and beyond northeastern Tibet: Geology, v. 38, no. 3, p. 223–226, https://doi.org/10.1130/G30711.1.

Duvall, A.R., Clark, M.K., van der Pluijm, B.A., and Li, C., 2011, Direct dating of Eocene reverse faulting in northeastern Tibet using Ar-dating of fault clays and low temperature thermochronometry: Earth and Planetary Science Letters, v. 304, no. 3–4, p. 520–526, https://doi.org/10.1016/j.epsl.2011.02.028.

Duvall, A.R., Clark, M.K., Kirby, E., Farley, K.A., Craddock, W.H., Li, C., and Yuan, D.Y., 2013, Low-temperature thermochronometry along the Kunlun and Haiyuan Faults, NE Tibetan Plateau: Evidence for kinematic change during late-stage orogenesis: Tectonics, v. 32, no. 5, p. 1190–1211, https://doi.org/10.1002/tect.20072.

England, P., and Houseman, G., 1986, Finite strain calculations of continental deformation: 2. Comparison with the India-Asia collision zone: Journal of Geophysical Research. Solid Earth, v. 91, no. B3, p. 3664–3676, https://doi.org/10.1029/JB091iB03p03664.

England, P., and Houseman, G., 1989, Extension during continental convergence, with application to the Tibetan Plateau: Journal of Geophysical Research. Solid Earth, v. 94, no. B12, p. 17,561–17,579, https://doi.org/10.1029/JB094iB12p17561.

Fang, X., Zhang, W., Meng, Q., Gao, J., Wang, X., King, J., Song, C., Dai, S., and Miao, Y., 2007, High-resolution magnetostratigraphy of the Neogene Huaitoutala section in the eastern Qaidam basin on the NE Tibetan plateau, Qinghai province, China and its implication on tectonic uplift of the NE Tibetan plateau: Earth and Planetary Science Letters, v. 258, p. 293–306, https://doi.org/10.1016/j.epsl.2007.03.042.

Flowers, R.M., Farley, K.A., and Ketcham, R.A., 2015, A reporting protocol for thermochronologic modeling illustrated with data from the Grand Canyon: Earth and Planetary Science Letters, v. 432, p. 425–435, https://doi.org/10.1016/j.epsl.2015.09.053.

Fu, B., and Awata, Y., 2007, Displacement and timing of left-lateral faulting in the Kunlun Fault Zone, northern Tibet, inferred from geologic and geomorphic features: Journal of Asian Earth Sciences, v. 29, no. 2–3, p. 253–265, https://doi.org/10.1016/j.jseaes.2006.03.004.

Galbraith, R.F., 1990, The radial plot: Graphical assessment of spread in ages: International Journal of Radiation Applications and Instrumentation. Part D. Nuclear Tracks and Radiation Measurements, v. 17, no. 3, p. 207–214, https://doi.org/10.1016/1359-0189(90)90036-W.

Gallagher, K., 2012, Transdimensional inverse thermal history modeling for quantitative thermochronology: Journal of Geophysical Research. Solid Earth, v. 117, no. B2, https://doi.org/10.1029/2011JB008825.

Gao, R., Wang, H., Yin, A., Dong, S., Kuang, Z., Zuza, A.V., Li, W., and Xiong, X., 2013, Tectonic development of the northeastern Tibetan Plateau as constrained by high resolution deep seismic-reflection data: Lithosphere, v. 5, no. 6, p. 555–574, https://doi.org/10.1130/L293.1.

Gehrels, G.E., Yin, A., and Wang, X.F., 2003, Magmatic history of the Altyn Tagh, Nan Shan, and Qilian Shan region of western China: Journal of Geophysical Research. Solid Earth, v. 108, no. B9, https://doi.org/10.1029/2002JB001876.

George, A.D., Marshallsea, S.J., Wyrwoll, K.H., Chen, J., and Lu, Y., 2001, Miocene cooling in the northern Qilian Shan, northeastern margin of the Tibetan Plateau, revealed by apatite fission-track and vitrinite-reflectance analysis: Geology, v. 29, no. 10, p. 939–942, https://doi.org/10.1130/0091-7613(2001)029<0939:MCITNQ>2.0.CO;2.

Gleadow, A.J.W., and Brown, R.W., 2000, Fission track thermochronology and the long-term denudational response to tectonics, *in* Summerfield, M.A., ed., Geomorphology and Global Tectonics. New York, USA, John Wiley, p. 57–75.

Gleadow, A.J.W., Duddy, I.R., Green, P.F., and Lovering, J.F., 1986, Confined fission track lengths in apatite: A diagnostic tool for thermal history analysis: Contributions to Mineralogy and Petrology, v. 94, no. 4, p. 405–415, https://doi.org/10.1007/BF00376334.

Green, P.F., 1988, The relationship between track shortening and fission track age reduction in apatite: Combined influences of inherent instability, annealing anisotropy, length bias and system calibration: Earth and Planetary Science Letters, v. 89, no. 3–4, p. 335–352, https://doi.org/10.1016/0012-821X(88)90121-5.

Guo, A., Zhang, G., Qiang, J., Sun, T., Li, G., and Yao, A., 2009, Indosinian Zongwulong orogenic belt on the northeastern margin of the Qinghai-Tibet Plateau [in Chinese with English Abstract]: Acta Petrologica Sinaca, v. 25, no. 8, p. 1–12.

Hardy, S., and Ford, M., 1997, Numerical modeling of trishear fault propagation folding: Tectonics, v. 16, no. 5, p. 841–854, https://doi.org/10.1029/97TC01171.

He, C., Zhang, Y., Li, J., Li, H., Sun, D., and Xiong, J., 2019, Kinematics of the Maxian Mountain Fault, Northeastern Tibetan Plateau: the history of Cretaceous–Cenozoic sedimentary and Tectonic Deformation [in Chinese with English Abstract]: Acta Geoscientica Sinica, v. 40, no. 4, p. 563–587, https://doi.org/10.3975/cagsb.2018.111901.

He, P., Song, C., Wang, Y., Meng, Q., Chen, L., Yao, L., Huang, S., Feng, W., and Chen, S., 2018, Cenozoic deformation history of the Qilian Shan (northeastern Tibetan Plateau) constrained by detrital apatite fission track thermochronology in the northeastern Qaidam Basin: Tectonophysics, v. 749, no. 6, p. 1–11, https://doi.org/10.1016/j.tecto.2018.10.017.

Hilley, G.E., Strecker, M.R., and Ramos, V.A., 2004, Growth and erosion of fold-and-thrust belts with an application to the Aconcagua fold-and- thrust belt, Argentina: Journal of Geophysical Research. Solid Earth, v. 109, no. B1, https://doi.org/10.1029/2002JB002282.

Horton, B.K., and Schmitt, J.G., 1996, Sedimentology of a lacustrine fan-delta system, Miocene horse camp formation, Nevada, USA: Sedimentology, v. 43, no. 1, p. 133–155, https://doi.org/10.1111/j.1365-3091.1996.tb01464.x.

Hough, B.G., Garzione, C.N., Wang, Z., Lease, R.O., Burbank, D.W., and Yuan, D., 2011, Stable isotope evidence for topographic growth and basin segmentation: Implications for the evolution of the NE Tibetan Plateau: Geological Society of America Bulletin, v. 123, no. 1–2, p. 168–185, https://doi.org/10.1130/B30090.1.

Hu, X., Garzanti, E., Moore, T., and Raffi, I., 2015, Direct stratigraphic dating of India-Asia collision onset at the Selandian (middle Paleocene, 59 ± 1 Ma): Geology, v. 43, no. 10, p. 859–862, https://doi.org/10.1130/G36872.1.

Hu, X., Garzanti, E., Wang, J., Huang, W., An, W., and Webb, A., 2016, The timing of India-Asia collision onset: Facts, theories, controversies: Earth-Science Reviews, v. 160, p. 264–299, https://doi.org/10.1016/j.earscirev.2016.07.014.

Huang, X., Gao, R., Li, W., and Xiong, X., 2021, Seismic reflection evidence of crustal duplexing and lithospheric underthrusting beneath the western Qilian mountains, northeastern margin of the Tibetan Plateau: Science China. Earth Sciences, v. 64, no. 1, p. 96–109, https://doi.org/10.1007/s11430-020-9677-y.

Hurford, A.J., 1990, Standardization of fission track dating calibration: Recommendation by the Fission Track Working Group of the IUGS Subcommission on Geochronology: Chemical Geology. Isotope Geoscience Section, v. 80, p. 171–178, https://doi.org/10.1016/0168-9622(90)90025-8.

Ingersoll, R.V., Bullard, T.F., Ford, R.L., Grimm, J.P., Pickle, J.D., and Sares, S.W., 1984, The effect of grain size on detrital modes: A test of the Gazzi-Dickinson point-counting method: Journal of Sedimentary Petrology, v. 54, p. 103–116.

Ji, J., Zhang, K., Clift, P.D., Zhuang, G., Song, B., Ke, X., and Xu, Y., 2017, High-resolution magnetostratigraphic study of the Paleogene-Neogene strata in the Northern Qaidam Basin: Implications for the growth of the Northeastern Tibetan Plateau: Gondwana Research, v. 46, p. 141–155, https://doi.org/10.1016/j.gr.2017.02.015.

Jiang, R.B., Chen, X.H., Dang, Y.Q., Yin, A., Wang, L.Q., Jiang, W.M., Wan, J.L., Li, L., and Wang, X.F., 2008, Apatite fission track evidence for two phases Mesozoic-Cenozoic thrust faulting in eastern Qaidam basin [in Chinese with English Abstract]: Chinese Journal of Geophysics, v. 51, p. 117–125.

Jolivet, M., Brunel, M., Seward, D., Xu, Z., Yang, J., Roger, F., and Wu, C., 2001, Mesozoic and Cenozoic tectonics of the northern edge of the Tibetan Plateau: Fission-track constraints: Tectonophysics, v. 343, no. 1–2, p. 111–134, https://doi.org/10.1016/S0040-1951(01)00196-2.

Kapp, P., DeCelles, P.G., Gehrels, G.E., Heizler, M., and Ding, L., 2007, Geological records of the Lhasa-Qiangtang and Indo-Asian collisions in the Nima area of central Tibet: Geological Society of America Bulletin, v. 119, no. 7–8, p. 917–933, https://doi.org/10.1130/B26033.1.

Kapp, P., Pelletier, J.D., Rohrmann, A., Heermance, R., Russell, J., and Ding, L., 2011, Wind erosion in the Qaidam basin, Central Asia: Implications for tectonics, paleoclimate, and the source of the Loess Plateau: GSA Today, v. 21, no. 4/5, p. 4–10, https://doi.org/10.1130/GSATG99A.1.

Ke, X., Ji, J., Zhang, K., Kou, X., Song, B., and Wang, C., 2013, Magnetostratigraphy and anisotropy of magnetic susceptibility of the Lulehe Formation in the northeastern Qaidam Basin [English edition]: Acta Geologica Sinica, v. 87, no. 2, p. 576–587, https://doi.org/10.1111/1755-6724.12069.

Ketcham, R.A., 2005, Forward and inverse modeling of low temperature thermochronometry data: Reviews in Mineralogy and Geochemistry, v. 58, p. 275–314, https://doi.org/10.2138/rmg.2005.58.11.

Ketcham, R.A., Carter, A., Donelick, R.A., Barbarand, J., and Hurford, A.J., 2007, Improved modeling of fission-track annealing in apatite: The American Mineralogist, v. 92, no. 5–6, p. 799–810, https://doi.org/10.2138/am.2007.2281.

Lease, R.O., Burbank, D.W., Clark, M.K., Farley, K.A., Zheng, D., and Zhang, H., 2011, Middle Miocene reorganization of deformation along the northeastern Tibetan Plateau: Geology, v. 39, no. 4, p. 359–362, https://doi.org/10.1130/G31356.1.

Lease, R.O., Burbank, D.W., Hough, B., Wang, Z., and Yuan, D., 2012, Pulsed Miocene range growth in northeastern Tibet: Insights from Xunhua Basin magnetostratigraphy and provenance: Geological Society of America Bulletin, v. 124, no. 5–6, p. 657–677, https://doi.org/10.1130/B30524.1.

Li, B., Chen, X., Zuza, A.V., Hu, D., Ding, W., Huang, P., and Xu, S., 2019, Cenozoic cooling history of the North Qilian Shan, northern Tibetan Plateau, and the initiation of the Haiyuan fault: Constraints from apatite-and zircon-fission track thermochronology: Tectonophysics, v. 751, p. 109–124, https://doi.org/10.1016/j.tecto.2018.12.005.

Li, B., Zuza, A.V., Chen, X., Hu, D., Shao, Z., Qi, B., Wang, Z., Levy, D.A., and Xiong, X., 2020, Cenozoic multiphase deformation in the Qilian Shan and out-of-sequence development of the northern Tibetan Plateau: Tectonophysics, v. 782–783, https://doi.org/10.1016/j.tecto.2020.228423.

Li, B., Zuza, A.V., Chen, X., Wang, Z.-Z., Shao, Z., Levy, D.A., Wu, C., Xu, S., and Sun, Y., 2021, Pre-Cenozoic evolution of the northern Qilian Orogen from zircon geochronology: Framework for early growth of the northern Tibetan Plateau: Palaeogeography, Palaeoclimatology, Palaeoecology, v. 562, https://doi.org/10.1016/j.palaeo.2020.110091.

Li, L., Garzione, C.N., Pullen, A., and Chang, H., 2016, Early-middle Miocene topographic growth of the northern Tibetan Plateau: Stable isotope and sedimentation evidence from the southwestern Qaidam basin: Palaeogeography, Palaeoclimatology, Palaeoecology, v. 461, p. 201–213, https://doi.org/10.1016/j.palaeo.2016.08.025.

Lin, X., Chen, H., Wyrwoll, K.H., Batt, G.E., Liao, L., and Xiao, J., 2011, The uplift history of the Haiyuan-Liupan Shan region northeast of the present Tibetan Plateau: Integrated constraint from stratigraphy and thermochronology: The Journal of Geology, v. 119, no. 4, p. 372–393, https://doi.org/10.1086/660190.

Lin, X., Wyrwoll, K.H., Chen, H., and Cheng, X., 2016, On the timing and forcing mechanism of a mid-Miocene arid climate transition at the NE margins of the Tibetan Plateau: Stratigraphic and sedimentologic evidence from the Sikouzi Section: International Journal of Earth Sciences, v. 105, no. 3, p. 1039–1049, https://doi.org/10.1007/s00531-015-1213-z.

Liu, D., Li, H., Sun, Z., Pan, J., Wang, M., and Wang, H., 2017, AFT dating constrains the Cenozoic uplift of the Qimen Tagh Mountains, Northeast Tibetan Plateau, comparison with LA-ICPMS Zircon U-Pb ages: Gondwana Research, v. 41, p. 438–450, https://doi.org/10.1016/j.gr.2015.10.008.

Liu, R., Chen, Y., Yu, X., Du, W., Cheng, X., and Guo, Z., 2019a, An analysis of distributed strike-slip shear deformation of the Qaidam Basin, northern Tibetan Plateau: Geophysical Research Letters, v. 46, no. 8, p. 4202–4211, https://doi.org/10.1029/2018GL081523.

Liu, C., Wu, C., Song, Z., Liu, W., and Zhang, H., 2019b, Petrogenesis and tectonic significance of Early Paleozoic magmatism in the northern margin of the Qilian block, northeastern Tibetan Plateau: Lithosphere, v. 11, no. 3, p. 365–385, https://doi.org/10.1130/L1047.1.

Liu, Q., Li, Y., Xiong, J., Zhang, H., Ge, W., Zhao, X., Huang, F., Hu, X., Zhong, Y., and Xin, W., 2021, Late Quaternary steady deformation of the Minle Fault in the north Qilian Shan, NE Tibet: Tectonophysics, v. 807, https://doi.org/10.1016/j.tecto.2021.228775.

Liu, Y., Tan, X., Ye, Y., Zhou, C., Lu, R., Murphy, M.A., Xu, X., and Suppe, J., 2020, Role of erosion in creating thrust recesses in a critical-taper wedge: An example from Eastern Tibet: Earth and Planetary Science Letters, v. 540, https://doi.org/10.1016/j.epsl.2020.116270.

Lu, H.J., and Xiong, S.F., 2009, Magnetostratigraphy of the Dahonggou section, northern Qaidam Basin and its bearing on Cenozoic tectonic evolution of the Qilian Shan and Altyn Tagh Fault: Earth and Planetary Science Letters, v. 288, p. 539–550, https://doi.org/10.1016/j.epsl.2009.10.016.

Lu, H., Wang, E., Shi, X., and Meng, K., 2012, Cenozoic tectonic evolution of the Elashan range and its surroundings, northern Tibetan Plateau, as constrained by paleomagnetism and apatite fission track analyses: Tectonophysics, v. 580, p. 150–161, https://doi.org/10.1016/j.tecto.2012.09.013.

Lu, Y., Fang, X., Appel, E., Wang, J., Herb, C., Han, W., Wu, F., and Song, C., 2015, A 7.3–1.6 Ma grain size record of interaction between anticline uplift and climate change in the western Qaidam Basin, NE Tibetan Plateau: Sedimentary Geology, v. 319, no. 15, p. 40–51, https://doi.org/10.1016/j.sedgeo.2015.01.008.

Malavieille, J., 2010, Impact of erosion, sedimentation, and structural heritage on the structure and kinematics of orogenic wedges: Analog models and case studies: GSA Today, v. 20, no. 1, p. 4–10, https://doi.org/10.1130/GSATG48A.1.

McQuarrie, N., Ehlers, T.A., Barnes, J.B., and Meade, B., 2008, Temporal variation in climate and tectonic coupling in the central Andes: Geology, v. 36, no. 12, p. 999–1002, https://doi.org/10.1130/G25124A.1.

McRivette, M.W., Yin, A., Chen, X.H., and Gehrels, G.E., 2019, Cenozoic basin evolution of the central Tibetan plateau as constrained by U-Pb detrital zircon geochronology, sandstone petrology, and fission-track thermochronology: Tectonophysics, v. 751, p. 150–179, https://doi.org/10.1016/j.tecto.2018.12.015.

Meng, Q., and Fang, X., 2008, Cenozoic tectonic development of the Qaidam Basin in the northeastern Tibetan Plateau, *in* Meng, Q.-R., and Fang, X., eds., Investigations into the Tectonics of the Tibetan Plateau: Geological Society of America Special Papers, v. 444, p. 1–24, https://doi.org/10.1130/2008.2444(01).

Meyers, J.H., Suttner, L.J., Furer, L.C., May, M.T., and Soreghan, M.J., 1992, Intrabasinal tectonic control on fluvial sandstone bodies in the Cloverly Formation (Early Cretaceous), west-Central Wyoming, USA: Basin Research, v. 4, p. 315–335, https://doi.org/10.1111/j.1365-2117.1992.tb00051.x.

Meyer, B., Tapponnier, P., Bourjot, L., Métivier, F., Gaudemer, Y., Peltzer, G., Shunmin, G., and Zhitai, C., 1998, Crustal thickening in Gansu-Qinghai, lithospheric mantle subduction, and oblique, strike-slip controlled growth of the Tibet Plateau: Geophysical Journal International, v. 135, p. 1–47, https://doi.org/10.1046/j.1365-246X.1998.00567.x.

Molnar, P., England, P., and Martinod, J., 1993, Mantle dynamics, uplift of the Tibetan Plateau, and the Indian monsoon: Reviews of Geophysics, v. 31, no. 4, p. 357–396, https://doi.org/10.1029/93RG02030.

Molnar, P., and Stock, J.M., 2009, Slowing of India's convergence with Eurasia since 20 Ma and its implications for Tibetan mantle dynamics: Tectonics, v. 28, no. 3, TC3001, https://doi.org/10.1029/2008TC002271.

Nie, J., Ren, X., Saylor, J. E., Su, Q., Horton, B. K., Bush, M. A., Chen, W., and Pfaff, K., 2020, Magnetic polarity stratigraphy, provenance, and paleoclimate analysis of Cenozoic strata in the Qaidam Basin, NE Tibetan Plateau: Geological Society of America Bulletin, v. 132, no. 1–2, p. 310–320, https://doi.org/10.1130/B35175.1.

Pang, J., Yu, J., Zheng, D., Wang, W., Ma, Y., Wang, Y., et al., 2019, Neogene expansion of the Qilian Shan, north Tibet: Implications for the dynamic evolution of the Tibetan Plateau: Tectonics, v. 38, p. 1018–1032, https://doi.org/10.1029/2018TC005258.

Pei, Y., Paton, D., Wu, K., and Xie, L., 2017, Subsurface structural interpretation by applying trishear algorithm: An example from the Lenghu5 fold-and-thrust belt, Qaidam Basin, Northern Tibetan Plateau: Journal of Asian Earth Sciences, v. 143, p. 343–353, https://doi.org/10.1016/j.jseaes.2017.05.012.

Qi, B., Hu, D., Yang, X., Zhang, Y., Tan, C., Zhang, P., and Feng, C., 2016, Apatite fission track evidence for the Cretaceous-Cenozoic cooling history of the Qilian Shan (NW China) and for stepwise northeastward growth of the northeastern Tibetan Plateau since early Eocene: Journal of Asian Earth Sciences, v. 124, p. 28–41, https://doi.org/10.1016/j.jseaes.2016.04.009.

Qinghai Bureau of Geology and Mineral Resources (BGMR), 1991, Regional Geology of Qinghai Province: Beijing, China, Geological Publishing House, 662 p.

Rieser, A.B., Neubauer, F., Liu, Y., and Ge, X., 2005, Sandstone provenance of northwestern sectors of the intracontinental Cenozoic Qaidam basin, western China: Tectonic vs. climatic control: Sedimentary Geology, v. 177, p. 1–18, https://doi.org/10.1016/j.sedgeo.2005.01.012.

Rieser, A.B., Liu, Y., Genser, J., Neubauer, F., Handler, R., Friedl, G., and Ge, X.H., 2006, $^{40}Ar/^{39}Ar$ ages of detrital white mica constrain the Cenozoic development of the intracontinental Qaidam Basin, China: Geological Society of America Bulletin, v. 118, p. 1522–1534, https://doi.org/10.1130/B25962.1.

Royden, L.H., Burchfel, B.C., and van der Hilst, R.D., 2008, The geological evolution of the Tibetan Plateau: Science, v. 321, p. 1054–1058, https://doi.org/10.1126/science.1155371.

Ryan, W.B.F., Carbotte, S.M., Coplan, J.O., O'Hara, S., Melkonian, A., Arko, R., Weissel, R.A., Ferrini, V., Goodwillie, A., Nitsche, F., Bonczkowski, J., and Zemsky, R., 2009, Global multi-resolution topography synthesis: Geochemistry, Geophysics, Geosystems, v. 10, no. 2009, Q03014, https://doi.org/10.1029/2008GC002332.

Sobel, E.R., Chen, J., and Heermance, R.V., 2006, Late Oligocene Early Miocene initiation of shortening in the Southwestern Chinese Tian Shan: Implications for Neogene shortening rate variations: Earth and Planetary Science Letters, v. 247, p. 70–81, https://doi.org/10.1016/j.epsl.2006.03.048.

Song, S.G., Niu, Y., Su, L., and Xia, X., 2013, Tectonics of the North Qilian orogen, NW China: Gondwana Research, v. 23, no. 4, p. 1378–1401, https://doi.org/10.1016/j.gr.2012.02.004.

Sun, J., Zhu, R., and An, Z., 2005, Tectonic uplift in the northern Tibetan Plateau since 13.7 Ma ago inferred from molasse deposits along the Altyn Tagh Fault: Earth and Planetary Science Letters, v. 235, no. 3–4, p. 641–653, https://doi.org/10.1016/j.epsl.2005.04.034.

Sun, Z., Feng, X., Li, D., Yang, F., Qu, Y., and Wang, H., 1999, Cenozoic Ostracoda and palaeoenvironments of the northeastern Tarim basin, western China: Palaeogeography, Palaeoclimatology, Palaeoecology, v. 148, p. 37–50, https://doi.org/10.1016/S0031-0182(98)00174-6.

Tapponnier, P., Peltzer, G., Le Dain, A.Y., Armijo, R., and Cobbold, P., 1982, Propagating extrusion tectonics in Asia: New insights from simple experiments with plasticine: Geology, v. 10, no. 12, p. 611–616, https://doi.org/10.1130/0091-7613(1982)10<611:PETIAN>2.0.CO;2.

Tapponnier, P., Zhiqin, X., Roger, F., Meyer, B., Arnaud, N., Wittlinger, G., and Jingsui, Y., 2001, Oblique stepwise rise and growth of the Tibet Plateau: Science, v. 294, no. 5547, p. 1671–1677, https://doi.org/10.1126/science.105978.

Vermeesch, P., 2009, RadialPlotter: A Java application for fission track, luminescence and other radial plots: Radiation Measurements, v. 44, p. 409–410, https://doi.org/10.1016/j.radmeas.2009.05.003.

Vincent, S.J., and Allen, M.B., 1999, Evolution of the Minle and Chaoshui Basins, China: Implications for Mesozoic strike-slip basin formation in Central Asia: Geological Society of America Bulletin, v. 111, no. 5, p. 725–742, https://doi.org/10.1130/0016-7606(1999)111<0725:EOTMAC>2.3.CO;2.

Wan, J., Zheng, D., Zheng, W., and Wang, W., 2011, Modeling thermal history during low temperature by K-feldspar MDD and fission track: Example from Meso-Cenozoic tectonic evolution in Saishiteng Shan in the northern margin of Qaidam Basin [in Chinese with English abstract]: Dizhen Dizhi, v. 33, no. 2, p. 369–382, https://doi.org/10.3969/j.issn.0253-4967.2011.02.010.

Wang, C.S., Zhao, X.X., Liu, Z.F., Lippert, P.C., Graham, S.A., Coe, R.S., Yi, H.S., Zhu, L.D., Liu, S., and Li, Y.L., 2008, Constrains on the early uplift history of the Tibetan Plateau: Proceedings of the National Academy of Sciences of the United States of America,

v. 105, p. 4987–4992, https://doi.org/10.1073/pnas.0703595105.

Wang, C.S., Dai, J.G., Zhao, X.X., Li, Y.L., Graham, S.A., He, D.F., Ran, B., and Meng, J., 2014, Outward growth of the Tibetan Plateau during the Cenozoic: A review: Tectonophysics, v. 621, p. 1–43, https://doi.org/10.1016/j.tecto.2014.01.036.

Wang, E., and Burchfiel, B.C., 2004, Late Cenozoic right-lateral movement along the Wenquan fault and associated deformation: Implications for the kinematic history of the Qaidam Basin, northeastern Tibetan Plateau: International Geology Review, v. 46, no. 10, p. 861–879, https://doi.org/10.2747/0020-6814.46.10.861.

Wang, E., Xu, F.Y., Zhou, J.X., Wan, J.L., and Burchfiel, B.C., 2006, Eastward migration of the Qaidam basin and its implications for Cenozoic evolution of the Altyn Tagh fault and associated river systems: Geological Society of America Bulletin, v. 118, p. 349–365, https://doi.org/10.1130/B25778.1.

Wang, F., Lo, C.H., Li, Q., Yeh, M.W., Wan, J., Zheng, D., and Wang, E., 2004, Onset timing of significant unroofing around Qaidam basin, northern Tibet, China: Constraints from $^{40}Ar/^{39}Ar$ and FT thermochronology on granitoids: Journal of Asian Earth Sciences, v. 24, p. 59–69, https://doi.org/10.1016/j.jseaes.2003.07.004.

Wang, F., Feng, H., Shi, W., Zhang, W., Wu, L., Yang, L., Wang, Y., Zhang, Z., and Zhu, R., 2016b, Relief history and denudation evolution of the northern Tibet margin: Constraints from $^{40}Ar/^{39}Ar$ and (U-Th)/He dating and implications for far-field effect of rising plateau: Tectonophysics, v. 675, p. 196–208, https://doi.org/10.1016/j.tecto.2016.03.001.

Wang, L., Cheng, F., Zuza, A. V., Jolivet, M., Liu, Y., Guo, Z., Li, X., and Zhang, C., 2021b, Diachronous growth of the northern Tibetan Plateau derived from flexural modeling: Geophysical Research Letters, v. 48, no. 8, https://doi.org/10.1029/2020GL092346.

Wang, W., Zhang, P., Pang, J., Garzione, C., Zhang, H., Liu, C., Zheng, D., Zheng, W., and Yu, J., 2016a, The Cenozoic growth of the Qilian Shan in the northeastern Tibetan Plateau: a sedimentary archive from the Jiuxi Basin: Journal of Geophysical Research. Solid Earth, v. 121, no. 4, p. 2235–2257, https://doi.org/10.1002/2015JB012689.

Wang, W.T., Zheng, W.J., Zhang, P.Z., Li, Q., Kirby, E., Yuan, D.Y., Zheng, D.W., Liu, C.C., Wang, Z.C., Zhang, H.P., and Pang, J.Z., 2017, Expansion of the Tibetan Plateau during the Neogene: Nature Communications, v. 8, https://doi.org/10.1038/ncomms15887.

Wang, W., Zheng, D., Li, C., Wang, Y., Zhang, Z., Pang, J., Wang, Y., Yu, J., Wang, Y., Zheng, W., Zhang, H., and Zhang, P., 2020, Cenozoic exhumation of the Qilian Shan in the northeastern Tibetan Plateau: Evidence from low-temperature thermochronology: Tectonics, v. 39, no. 4, https://doi.org/10.1029/2019TC005705.

Wang, X., Qiu, Z., Li, Q., Wang, B., Qiu, Z., and Meng, Q., 2007, Vertebrate paleontology, biostratigraphy, geochronology, and paleoenvironment of Qaidam Basin in northern Tibetan Plateau: Palaeogeography, Palaeoclimatology, Palaeoecology, v. 254, p. 363–385, https://doi.org/10.1016/j.palaeo.2007.06.007.

Wang, Y., Cheng, X., Zhang, Y., Yin, Z., Zuza, A., Yin, A., Wang, Y., Ding, W., Xu, S., Zhang, Y., Li, B., and Shao, Z., 2021a, Superposition of Cretaceous and Cenozoic deformation in northern Tibet: A far-field response to the tectonic evolution of the Tethyan orogenic system: Geological Society of America Bulletin, v. 134, p. 501–525, https://doi.org/10.1130/B35944.1.

Wang, Y., Chen, X., Shao, Z., Yu, W., and Su, H., 2021c, Miocene evolution of the basin-mountain system and paleogeomorphic reconstruction in the easternmost Qaidam Basin: Acta Geoscientica Sinica, v. 42, no. 1, p. 43–54, https://doi.org/10.3975/cagsb.2020.062901.

Wei, Y., Xiao, A., Wu, L., Mao, L., Zhao, H., Shen, Y., and Wang, L., 2016, Temporal and spatial patterns of Cenozoic deformation across the Qaidam Basin, Northern Tibetan Plateau: Terra Nova, v. 28, no. 6, p. 409–418, https://doi.org/10.1111/ter.12234.

Wu, C., Zuza, A.V., Chen, X., Ding, L., Levy, D.A., Liu, C., Liu, W., Jiang, T., and Stockli, D.F., 2019a, Tectonics of the Eastern Kunlun Range: Cenozoic reactivation of a Paleozoic-Early Mesozoic orogen: Tectonics, v. 38, p. 1609–1650, https://doi.org/10.1029/2018TC005370.

Wu, C., Zuza, A.V., Zhou, Z.G., Yin, A., McRivette, M.W., Chen, X.H., Ding, L., and Geng, J.Z., 2019c, Mesozoic-Cenozoic evolution of the Eastern Kunlun Range, central Tibet, and implications for basin evolution during the Indo-Asian collision: Lithosphere, v. 11, no. 4, p. 524–550, https://doi.org/10.1130/L1065.1.

Wu, L., Xiao, A., Wang, L., Shen, Z., Zhou, S., Chen, Y., Wang, L., Liu, D., and Guan, J., 2011, Late Jurassic-Early Cretaceous Northern Qaidam Basin, NW China: Implications for the earliest Cretaceous intracontinental tectonism: Cretaceous Research, v. 32, no. 4, p. 552–564, https://doi.org/10.1016/j.cretres.2011.04.002.

Wu, L., Xiao, A., Yang, S., Wang, L., Mao, L., Wang, L., Dong, Y., and Xu, B., 2012, Two-stage evolution of the Altyn Tagh Fault during the Cenozoic: New insight from provenance analysis of a geological section in NW Qaidam Basin, NW China: Terra Nova, v. 24, no. 5, p. 387–395, https://doi.org/10.1111/j.1365-3121.2012.01077.x.

Wu, L., Xiao, A., Ma, D., Li, H., Xu, B., Shen, Y., and Mao, L., 2014, Cenozoic fault systems in southwest Qaidam Basin, northeastern Tibetan Plateau: Geometry, temporal development, and significance for hydrocarbon accumulation: AAPG Bulletin, v. 98, no. 6, p. 1213–1234, https://doi.org/10.1306/11131313087.

Wu, L., Lin, X., Cowgill, E., Xiao, A., Cheng, X., Chen, H., Zhao, H., Shen, Y., and Yang, S., 2019b, Middle Miocene reorganization of the Altyn Tagh fault system, northern Tibetan Plateau: Geological Society of America Bulletin, v. 131, no. 7-8, p. 1157–1178, https://doi.org/10.1130/B31875.1.

Wu, M., Zhuang, G., Hou, M., and Liu, Z., 2021, Expanded lacustrine sedimentation in the Qaidam Basin on the northern Tibetan Plateau: Manifestation of climatic wetting during the Oligocene icehouse: Earth and Planetary Science Letters, v. 565, https://doi.org/10.1016/j.epsl.2021.116935.

Xia, W., Zhang, N., Yuan, X., Fan, L., and Zhang, B., 2001, Cenozoic Qaidam basin, China: A stronger tectonic inversed, extensional rifted basin: The American Association of Petroleum Geologists Bulletin, v. 85, p. 715–736.

Yan, Z., Fu, C., Aitchison, J.C., Buckman, S., Niu, M., Cao, B., Sun, Y., Guo, X., Wang, Z., and Zhou, R., 2019, Retro-foreland basin development in response to Proto-Tethyan Ocean closure, NE Tibet Plateau: Tectonics, https://doi.org/10.1029/2019TC005560.

Yang, F., Ma, Z., Xu, T., and Ye, S., 1992, A Tertiary paleomagnetic stratigraphic profile in Qaidam basin: Yanshi Xuebao, v. 13, p. 97–101.

Yang, J.S., Xu, Z., Zhang, J., Chu, C.Y., Zhang, R., and Liou, J.G., 2001, Tectonic significance of early Paleozoic high-pressure rocks in Altun-Qaidam-Qilian Mountains, northwest China, *in* Hendric, M.S., and Davis, G.A., eds., Paleozoic and Mesozoic Tectonic Evolution of Central Asia: From Continental Assembly to Intracontinental Deformation: Geological Society of America Memoir 194, p. 151–170, https://doi.org/10.1130/0-8137-1194-0.151.

Yang, J., Xu, Z., Zhang, J., Song, S., Wu, C., Shi, R., Li, H., and Brunel, M., 2002, Early Paleozoic North Qaidam UHP metamorphic belt on the north-eastern Tibetan plateau and a paired subduction model: Terra Nova, v. 14, no. 5, p. 397–404, https://doi.org/10.1046/j.1365-3121.2002.00438.x.

Yin, A., 2010, Cenozoic tectonic evolution of Asia: A preliminary synthesis: Tectonophysics, v. 488, p. 293–325, https://doi.org/10.1016/j.tecto.2009.06.002.

Yin, A., Rumelhart, P.E., Butler, R., Cowgill, E., Harrison, T.M., Foster, D.A., Ingersoll, R.V., Qing, Z., Xian-Qiang, Z., Xiao-Feng, W., Hanson, A., and Raza, A., 2002, Tectonic history of the Altyn Tagh fault system in northern Tibet inferred from Cenozoic sedimentation: Geological Society of America Bulletin, v. 114, no. 10, p. 1257–1295, https://doi.org/10.1130/0016-7606(2002)114<1257:THOTAT>2.0.CO;2.

Yin, A., Dang, Y., Zhang, M., McRivette, M.W., Burgess, W.P., and Chen, X., 2007, Cenozoic tectonic evolution of Qaidam basin and its surrounding regions (part 2): Wedge tectonics in southern Qaidam basin and the Eastern Kunlun Range, *in* Sears, J.W., Harms, T.A., and Evenchick, C.A., eds., Whence the Mountains? Inquiries into the Evolution of Orogenic Systems: A Volume in Honor of Raymond A. Price: Geological Society of America Special Paper 433, 369–390, https://doi.org/10.1130/2007.2433(18).

Yin, A., Dang, Y.-Q., Wang, L.-C., Jiang, W.-M., Zhou, S.-P., Chen, X.-H., Gehrels, G.E., and McRivette, M.W., 2008a, Cenozoic tectonic evolution of Qaidam Basin and its surrounding regions (part 1): The southern Qilian Shan-Nan Shan thrust belt and northern Qaidam Basin: Geological Society of America Bulletin, v. 120, no. 7–8, p. 813–846, https://doi.org/10.1130/B26180.1.

Yin, A., Dang, Y.Q., Zhang, M., Chen, X.H., and McRivette, M.W., 2008b, Cenozoic tectonic evolution of the Qaidam Basin and its surrounding regions (Part 3): Structural geology, sedimentation, and regional tectonic reconstruction: Geological Society of America Bulletin, v. 120, no. 7–8, p. 847–876, https://doi.org/10.1130/B26232.1.

Yu, J., Zheng, D., Pang, J., Wang, Y., Fox, M., Vermeesch, P., Li, C., Xiao, L., Hao, Y., and Wang, Y., 2019a, Miocene range growth along the Altyn Tagh fault: Insights from apatite fission track and (U-Th)/He thermochronometry in the western Danghenan Shan, China: Journal of Geophysical Research. Solid Earth, v. 124, p. 9433–9453, https://doi.org/10.1029/2019JB017570.

Yu, J.X., Pang, J.Z., Wang, Y.Z., Zheng, D.W., Liu, C.C., Wang, W.T., Li, Y., Li, C., and Xiao, L., 2019b, Mid-Miocene uplift of the northern Qilian Shan as a result of the northward growth of the northern Tibetan Plateau: Geosphere, v. 15, no. 2, p. 423–432, https://doi.org/10.1130/GES01520.1.

Yu, L., Xiao, A., Wu, L., Tian, Y., Rittner, M., Lou, Q., and Pan, X., 2017a, Provenance evolution of the Jurassic northern Qaidam Basin (West China) and its geological implications: evidence from detrital zircon geochronology: International Journal of Earth Sciences, v. 106, p. 2713–2726, https://doi.org/10.1007/s00531-017-1455-z.

Yu, X., and Guo, Z., 2019, The role of base level, watershed attribute and sediment accumulation in the landscape and tectonic evolution of the Circum-Tibetan Plateau Basin and Orogen System: Journal of Asian Earth Sciences, v. 186, https://doi.org/10.1016/j.jseaes.2019.104053.

Yu, X., and Guo, Z., 2021, Surface uplift of the Tibetan Plateau: Constraints from isostatic effects of Cenozoic sedimentary accumulation: Journal of Asian Earth Sciences, v. 208, https://doi.org/10.1016/j.jseaes.2020.104662.

Yu, X., Huang, B., Guan, S., Fu, S., Cheng, F., Cheng, X., Zhang, T., and Guo, Z., 2014a, Anisotropy of magnetic susceptibility of Eocene and Miocene sediments in the Qaidam Basin, Northwest China: Implication for Cenozoic tectonic transition and depocenter migration: Geochemistry, Geophysics, Geosystems, v. 15, no. 6, p. 2095–2108, https://doi.org/10.1002/2014GC005231.

Yu, X., Fu, S., Guan, S., Huang, B., Cheng, F., Cheng, X., Zhang, T., and Guo, Z., 2014b, Paleomagnetism of Eocene and Miocene sediments from the Qaidam basin: Implication for no integral rotation since the Eocene and a rigid Qaidam block: Geochemistry, Geophysics, Geosystems, v. 15, no. 6, p. 2109–2127, https://doi.org/10.1002/2014GC005230.

Yu, X., Guo, Z., and Fu, S., 2015, Endorheic or exorheic: Differential isostatic effects of Cenozoic sediments on the elevations of the cratonic basins around the Tibetan Plateau: Terra Nova, v. 27, no. 1, p. 21–27, https://doi.org/10.1111/ter.12126.

Yu, X., Guo, Z., Zhang, Q., Cheng, X., Du, W., Wang, Z., and Bian, Q., 2017b, Denan Depression controlled by northeast-directed Olongbulak thrust zone in northeastern Qaidam Basin: Implications for growth of northern Tibetan Plateau: Tectonophysics, v. 717, p. 116–126, https://doi.org/10.1016/j.tecto.2017.06.017.

Yu, X., Guo, Z., Guan, S., Du, W., Wang, Z., Bian, Q., and Li, L., 2019c, Landscape and tectonic evolution of Bayin River watershed, northeastern Qaidam basin, and northern Tibetan Plateau: Implications for the role of river morphology in source analysis and low-temperature thermochronology: Journal of Geophysical Research. Earth Surface, v. 124, no. 7, p. 1701–1719, https://doi.org/10.1029/2018JF004989.

Yu, X., Guo, Z., Chen, Y., Du, W., Wang, Z., and Bian, Q., 2020, River system reformed by the Eastern Kunlun

Fault: Implications from geomorphological features in the Eastern Kunlun Mountains, Northern Tibetan Plateau: Geomorphology, v. 350, https://doi.org/10.1016/j.geomorph.2019.106876.

Yu, X., Guo, Z., Chen, Y., Cheng, X., Du, W., and Wang, Z., 2021a, Recognition and application of offlap in endorheic basins: new insights into plateau growth: International Geology Review, https://doi.org/10.1080/00206814.2021.1894611.

Yu, X., Guo, Z., Chen, Y., Du, W., and Wang, Z., 2021b, Coupling between surface processes and crustal deformation: Insights from the late Cenozoic development of the Qaidam Basin, China: Global and Planetary Change, v. 207, https://doi.org/10.1016/j.gloplacha.2021.103646.

Yuan, D.Y., Champagnac, J.D., Ge, W.P., Molnar, P., Zhang, P.Z., Zheng, W.J., Zhang, H.P., and Liu, X.W., 2011, Late Quaternary right-lateral slip rates of faults adjacent to the lake Qinghai, northeastern margin of the Tibetan Plateau: Geological Society of America Bulletin, v. 123, no. 9–10, p. 2016–2030, https://doi.org/10.1130/B30315.1.

Yuan, D.Y., Ge, W.P., Chen, Z.W., Li, C.Y., Wang, Z.C., and Roe, G.H., 2013, The growth of northeastern Tibet and its relevance to large-scale continental geodynamics: A review of recent studies: Tectonics, v. 32, p. 1358–1370, https://doi.org/10.1002/tect.20081.

Yuan, W.M., Zhang, X.T., Dong, J.Q., Tang, Y.H., Yu, F.S., and Wang, S.C., 2003, A new vision of the intracontinental evolution of the eastern Kunlun Mountains, Northern Qinghai-Tibet plateau, China: Radiation Measurements, v. 36, no. 1–6, p. 357–362, https://doi.org/10.1016/S1350-4487(03)00151-3.

Yue, Y., and Liou, J.G., 1999, Two-stage evolution model for the Altyn Tagh fault, China: Geology, v. 27, no. 3, p. 227–230, https://doi.org/10.1130/0091-7613(1999)027<0227:TSEMFT>2.3.CO;2.

Yue, Y.J., Graham, S.A., Ritts, B.D., and Wooden, J.L., 2005, Detrital zircon provenance evidence for large-scale extrusion along the Altyn Tagh Fault: Tectonophysics, v. 406, p. 165–178, https://doi.org/10.1016/j.tecto.2005.05.023.

Zhang, C., Wu, L., Chen, W., Zhang, Y., Xiao, A., Zhang, J., Chen, S., and Chen, H., 2020, Early Cretaceous foreland-like Northeastern Qaidam Basin, Tibetan Plateau and its tectonic implications: Insights from sedimentary investigations, detrital zircon U-Pb analyses and seismic profiling: Palaeogeography, Palaeoclimatology, Palaeoecology, v. 557, https://doi.org/10.1016/j.palaeo.2020.109912.

Zhang, H.P., Craddock, W.H., Lease, R.O., Wang, W.T., Yuan, D.Y., Zhang, P.Z., Molnar, P., Zheng, D.W., and Zheng, W.J., 2012, Magnetostratigraphy of the Neogene Chaka basin and its implications for mountain building processes in the north-eastern Tibetan Plateau: Basin Research, v. 24, p. 31–50, https://doi.org/10.1111/j.1365-2117.2011.00512.x.

Zhang, J.X., Yang, J.S., Mattinson, C.G., Xu, Z.Q., Meng, F.C., and Shi, R.D., 2005, Two contrasting eclogite cooling histories, North Qaidam HP/UHP terrane, western China: Petrological and isotopic constraints: Lithos, v. 84, p. 51–76, https://doi.org/10.1016/j.lithos.2005.02.002.

Zhang, Z.C., and Wang, X.S., 2004, The issues of application for the fission track dating and its geological significance [in Chinese with English abstract]: Beijing Da Xue Bao. Zi Ran Ke Xue Bao, v. 40, p. 895–905, https://doi.org/10.3321/j.issn:0479-8023.2004.06.007.

Zheng, D., Clark, M.K., Zhang, P., Zheng, W., and Farley, K.A., 2010, Erosion, fault initiation and topographic growth of the North Qilian Shan (northern Tibetan Plateau): Geosphere, v. 6, no. 6, p. 937–941, https://doi.org/10.1130/GES00523.1.

Zheng, D., Wang, W., Wan, J., Yuan, D., Liu, C., Zheng, W., Zhang, H., Pang, Z., and Zhang, P., 2017, Progressive northward growth of the northern Qilian Shan-Hexi Corridor (northeastern Tibet) during the Cenozoic: Lithosphere, v. 9, no. 3, p. 408–416, https://doi.org/10.1130/L587.1.

Zhou, J., Xu, F., Wang, T., Cao, A., and Yin, C., 2006, Cenozoic deformation history of the Qaidam Basin, NW China: Results from cross-section restoration and implications for Qinghai–Tibet Plateau tectonics: Earth and Planetary Science Letters, v. 243, no. 1–2, p. 195–210, https://doi.org/10.1016/j.epsl.2005.11.033.

Zhu, D.C., Wang, Q., Zhao, Z.D., Chung, S.L., Cawood, P.A., Niu, Y., Liu, S., Wu, F., and Mo, X.X., 2015, Magmatic record of India-Asia collision: Scientific Reports, v. 5, no. 1, p. 1–9, https://doi.org/10.1038/srep14289.

Zhuang, G., Hourigan, J.K., Ritts, B.D., and Kent-Corson, M.L., 2011, Cenozoic multiple-phase tectonic evolution of the northern Tibetan Plateau: Constraints from sedimentary records from Qaidam Basin, Hexi Corridor, and Subei Basin, northwest China: American Journal of Science, v. 311, no. 2, p. 116–152, https://doi.org/10.2475/02.2011.02.

Zhuang, G., Johnstone, S.A., Hourigan, J., Ritts, B., Robinson, A., and Sobel, E.R., 2018, Understanding the geologic evolution of northern Tibetan Plateau with multiple thermochronometers: Gondwana Research, v. 58, p. 195–210, https://doi.org/10.1016/j.gr.2018.02.014.

Zuza, A.V., and Yin, A., 2016, Continental deformation accommodated by non-rigid passive bookshelf faulting: An example from the Cenozoic tectonic development of northern Tibet: Tectonophysics, v. 677, p. 227–240, https://doi.org/10.1016/j.tecto.2016.04.007.

Zuza, A.V., Cheng, X., and Yin, A., 2016, Testing models of Tibetan Plateau formation with Cenozoic shortening estimates across the Qilian Shan–Nan Shan thrust belt: Geosphere, v. 12, no. 2, p. 501–532, https://doi.org/10.1130/GES01254.1.

Zuza, A.V., Wu, C., Reith, R.C., Yin, A., Li, J.H., Zhang, J.Y., Zhang, Y.X., Wu, L., and Liu, W.C., 2018, Tectonic evolution of the Qilian Shan: An early Paleozoic orogen reactivated in the Cenozoic: Geological Society of America Bulletin, v. 130, no. 5–6, p. 881–925, https://doi.org/10.1130/B31721.1.

Zuza, A.V., Wu, C., Wang, Z., Levy, D.A., Li, B., Xiong, X., and Chen, X., 2019, Underthrusting and duplexing beneath the northern Tibetan Plateau and the evolution of the Himalayan-Tibetan orogen: Lithosphere, v. 11, no. 2, p. 209–231, https://doi.org/10.1130/L1042.1.

Zuza, A.V., Gavillot, Y., Haproff, P.J., and Wu, C., 2020, Kinematic evolution of a continental collision: Constraining the Himalayan-Tibetan orogen via bulk strain rates: Tectonophysics, v. 797, https://doi.org/10.1016/j.tecto.2020.228642.

Science Editor: Wenjiao Xiao
Associate Editor: Yongjiang Liu

Manuscript Received 9 June 2021
Revised Manuscript Received 7 December 2021
Manuscript Accepted 20 February 2022

Printed in the USA